Alma Mater Studiorum · Università di Bologna

Scuola di Scienze
Dipartimento di Fisica e Astronomia
Corso di Laurea in Fisica

Radiation tolerance of novel organic flexible X-Ray detectors

Relatore:
Prof.ssa Beatrice Fraboni

Presentata da:
Sara Sacchi

Correlatore:
Dott.ssa Laura Basiricò

Correlatore:
Dott.ssa Ilaria Fratelli

Anno Accademico 2020/2021

"Sol crescentes decedens duplicat umbras"

Virgilio, Bucoliche II v.67

Contents

Sommario

I semiconduttori organici presentano numerose proprietà che li contraddistinguono dalla loro controparte inorganica. Il basso costo e la loro facilità di deposizione li rende ottimi candidati per lo sviluppo di una nuova generazione di rivelatori di radiazione ionizzante flessibile e scalabile su larga area. Altre caratteristiche avvalorano il loro possibile ruolo nei vari campi di applicazione medico, di fisica ad alte energie, sicurezza in aeroporto e installazioni nucleari o spaziali, quali la loro resistenza, leggerezza, flessibilità e la loro equivalenza ai tessuti umani in termini di assorbimento di fotoni ad alta energia. Alla base di questa tesi vi è lo studio e l'analisi di transistors organici a effetto di campo (OFET), con semiconduttore in TIPS e TIPGe -pentacene, come rivelatori di raggi X e la loro resistenza a danni al materiale e alla performance dovuti a esposizione a radiazione prolungata.

Abstract

Organic semiconductors exhibit numerous properties that distinguish them from their inorganic counterpart. Their low cost and ease of deposition make them excellent candidates for the development of a new generation of flexible and scalable large area ionizing radiation detectors. Other features support their possible role in various fields of medical application, high energy physics, airport security and nuclear or space installations, such as their strength, lightness, flexibility and their equivalence to human tissues in terms of high energy photon absorption. This thesis work is focused on the study and analysis of Organic Field Effect Transistors (OFET), with TIPS and TIPGe -pentacene semiconductors, as X-ray detectors and their resistance to material damage and performance due to prolonged radiation exposure.

Introduction

Ionizing radiation detectors cover a particularly relevant field of research and applications, from the social to the technological scopes: they are used in a wide range of activities, from microelectronics to industrial quality control, from sterilization to oil industry, from monitoring of nuclear waste to the conservation of cultural heritage and applications in the medical and space fields. One of their many possible approaches and studies is based on organic electronics, which in the last few decades has become a remarkable target of interest, as much on an academic level as on an industrial one.

The application of organic semiconductors into the field of ionizing radiation detection has given the opportunity to study and invest into a completely new, low-cost, lightweight and flexible electronics. The main differences between organic detectors and their rigid inorganic counterpart enabled these devices to be used into previously inconceivable fields, such as in the medical and space fields; in fact, they can now be easily worn thanks to their flexibility, non-toxicity and their equivalence to human tissues in terms of high energy photon absorption.

In recent times, fabrication techniques have been greatly improved. Organic semiconductors are now deposited from liquid phase, by low-cost, low energy requirement and relatively easy methods, allowing to cover large area and curved surfaces.

This thesis work is oriented to the study of ionizing radiation tolerance of organic field effect transistors (OFETs) as X-Ray direct detectors. Many benefits arise from the use of these devices as X-Ray detectors: primarily their integration ease into electronic circuits; secondly their peculiarity of being multi-terminal devices, which allows to vary the conductivity directly operating on the gate voltage; and, finally, their intrinsic amplification capacity.

In the first chapter, there is a first paragraph in which organic semiconductor and their deposition methods are explained and a second paragraph in which OFETs (Organic Field Effect Transistors) structure and functioning is addressed, as well as the explanation and exemplification of their characterization methods. Afterwards, basic notions of interaction between radiation and matter, the difference between direct and indirect radiation are introduced in relation to dosimeters and OFETs functioning. Finally, one last paragraph about the radiation hardness test, which is the one used for studying and analyzing radiation tolerance of examined OFETs.

The second chapter focuses on the examined OFETs fabrication, the experimental apparatus, the data collection of electrical and through X-Ray irradiation characterizations. Also, the radiation hardness study and the methods for extrapolating the fundamental parameters (mobility, threshold voltage V_{TH}, ON voltage V_{ON}, ON/OFF ratio, subthreshold swing slope S, photocurrent and sensitivity) are described, starting from the collecting data.

In the third chapter, the main results achieved during my work are reported and discussed for both the electrical characterization and X-Ray detection test.

Chapter 1

Ionizing radiation detectors based on Organic Field Effect Transistors

1.1 Organic semiconductors

The new research field of organic semiconductors has aroused more and more interest over the past few years. One of the most unique features of organic semiconductors is their easy manipulation.

Organic semiconductor materials are particularly efficient because they only form weak bonds, Van Der Waals bonds, which need a modest energetic input to be broken and re-formed. Since the required activation energy is less than that of covalent bonds, that allows them to be manipulated easily using a small energetic input. The electrical properties are due to conjugated p-orbitals, which facilitate electron delocalization and charge transport.

The weak intermolecular interaction allows using several techniques unavailable to covalently bonded thin film materials, such as thermal vacuum deposition and solution processing; unfortunately, due to the bond weakness, the structure of organic semiconductor layers can easily be disrupted. Several applications take advantage of the single deposition and patterning processes, ability to integrate with other devices and mechanical flexibility offered by the thin film format.

Different small molecules or polymers can be used for the fabrication of organic semiconductors; the most popular organic semiconductors so far are tetracene and pentacene (Fig.1.1).

They strongly organize to form polycrystalline films with good transport properties and they can also form large single crystals under appropriate conditions. Many small molecules have been functionalized to be soluble and deposited by solution, such as 6,13-Bis(triisopropylsilylethynyl)pentacene (TIPS-pentacene), which is particularly suitable to be deposited via solution. Processing these materials at or near room temperature will

lead the possibility to deposit them directly onto plastic substrates achieving mechanical flexible devices [1].

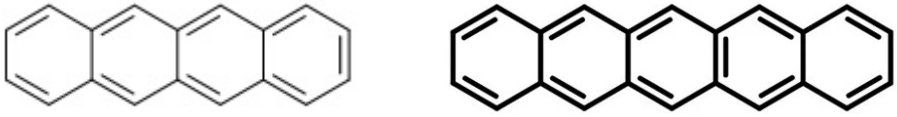

(a) Tetracene **(b)** Pentacene

Figure 1.1: Chemical structures of two among the most common organic semiconductor small molecules: (a) Tetracene molecule (b) Pentacene molecule.

There are some different techniques to deposit the organic semiconductor: thermal evaporation, deposition from solution or chemical vapor deposition for polymers. Deposition techniques from solution allow to process organic semiconductors at low temperature leading the possibility to develop flexible devices fabricated onto plastic substrates. Moreover, these techniques are easily scalable and they make possible to fabricate large-area devices.; they group different strategies of deposition which are more common, such as spin-coating, drop casting, dip coating, spray coating, blade coating and roll coating (Fig.1.2).

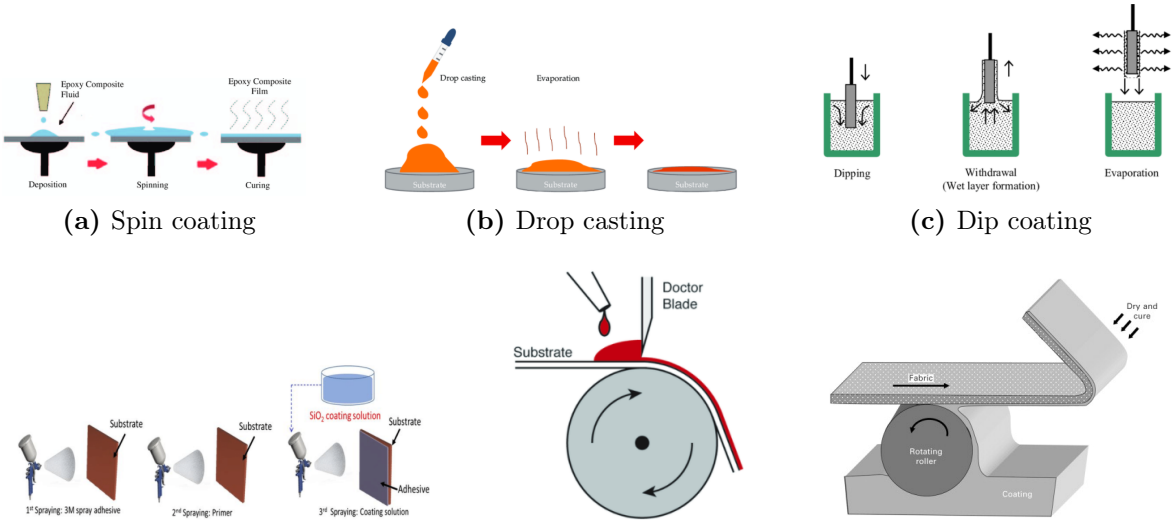

(a) Spin coating **(b)** Drop casting **(c)** Dip coating

(d) Spray coating **(e)** Blade coating **(f)** Roll coating

Figure 1.2: Some of the most employed deposition techniques for the organic semiconductor processing: (a) Spin coating [2] (b) Drop casting [3] (c) Dip coating [4] (d) Spray coating [5] (e) Blade coating [6] (f) Roll coating [7]

Printing processes are those that are amenable to large-area deposition with spatial deposition control and that do not primarily rely on meniscus-driven coating. Printing is a family of techniques that deposit and pattern a target at the same time, which includes ejected drop printing (thermal inkjet), stream dispensing, indirect and offset printing methods (Fig.1.3). The printing of polymer solutions, for example, to form precisely patterned arrays is relatively complex, requiring an understanding of the fluid flow involved [8].

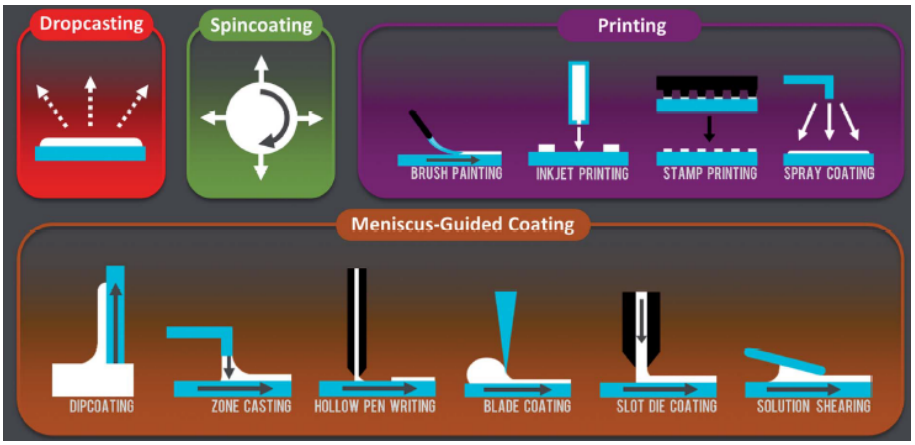

Figure 1.3: A schematic summary of the solution-based deposition techniques employed for organic semiconductors and discussed [8].

Otherwise, for the patterning of the device, photolithography is an efficient strategy; the device is exposed to a structured radiation pattern, such as UV through a high optical density mask, and developed. The only flaw of this technique is that many oligomeric materials are not tolerant to solvent exposure: pentacene is not soluble in any solvent and when exposed to most solvents their semiconductor character is destroyed. The solution is to protect the semiconductor from materials it is not compatible with.

1.2 Organic Field Effect Transistors

Over the past 30 years a new field of research has rapidly grown, organic materials and solution-based devices have been sophisticated and improved through new fabrication techniques to develop novel flexible technologies easily scalable onto large-areas. This development has led to the use of new organic semiconductors in various electronic devices, for instance in organic field effect thin film transistors (OFETs), in which the layer of the semiconductor is an organic thin film deposited from solution, characterized by mechanical flexibility, low-cost fabrication technique and simple processing. Organic

semiconductor materials can be synthesized and chemically tailored to reach specific properties, and this has justified their success in optoelectronic applications.

1.2.1 OFET's structure and working principles

These devices are built depositing electrically active layers of material one after another, forming three different electrodes dependently on the order in which the layers are deposited. Each layer plays a different role in the OFET constitution; dependently on the wanted configuration, the transistor structure changes and works differently. OFETs are multiterminal devices, having the gate electrode (G), the source electrode (S), the drain electrode (D); two other layers constitute the transistor structure: the gate dielectric and the semiconductor layer or active layer.

There can be four possible configurations: bottom gate bottom contacts (BGBC); bottom gate top contacts (BGTC); top gate bottom contacts (TGBC); and top gate top contacts (TGTC) (Fig.1.4). BGBC and TGTC are coplanar, where the electrodes of source and drain and the conductive channel are located on the same plane, while BGTC and TGBC are staggered, where the conductive channel is offset from the plane of the source and drain electrodes. The BGBC configuration allows a quicker examination of semiconductor materials because the gate, source, drain electrodes and the dielectric layer are pre-fabricated, and the semiconductor deposition is the last step. The only shortcoming is that the semiconductor is exposed to ambient conditions which may accelerate degradation [9].

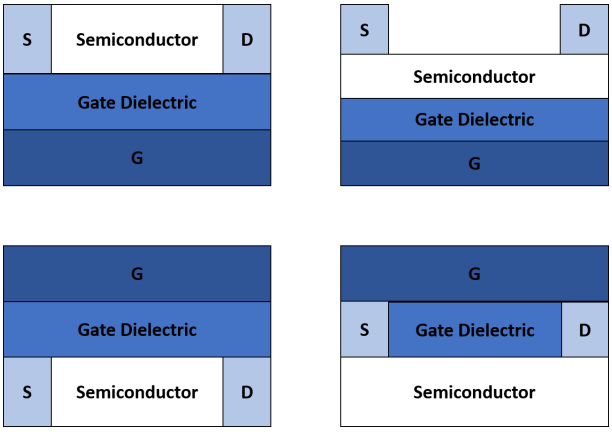

Figure 1.4: The four possible OFETs configurations: on the upper left the bottom gate bottom contact (BGBC), on the upper right the bottom gate top contact (BGTC), on the lower left the top gate bottom contact (TGBC) and on the lower right the top gate top contact configuration (TGTC).

OFET's functioning is based on the transport of charge in the organic semiconductor; the operation on the device relies on the application of one potential to the gate electrode

and another at the drain, keeping the source at ground. This results into two voltages, the gate-source voltage (V_{GS}), and the drain-source voltage (V_{DS}). In the case of ideal devices with no threshold voltage, the device is turned ON only if there is a V_{GS} applied at the gate. In this case, the V_{GS} polarizes the dielectric causing the accumulation of charge carriers at the semiconductor dielectric interface. There is a voltage at which the device begins accumulating charge, a threshold voltage V_{TH}; this is referred to as the gate voltage at which current begins to flow. The V_{TH} is needed to fill charge traps at the semiconductor-dielectric interface before free charge can accumulate [1]. The transistor can be a p-type or a n-type, dependently if the majority charge carriers are holes or electrons. An applied V_{DS} forces the accumulated charge carriers from the source to the drain electrode where the drain current I_{DS} is measured [9].

1.2.2 OFET's characterization

Electrical characterization

The selection of tests used to characterize a device needs to be motivated by the end application of the transistors in question. Electrical devices, as OFETs, must be electrically characterized. Having a complete electrical characterization means collecting and analyze two types of curves: the output and the transfer characteristics. The output characteristic shows the evolution of the drain current as a function of drain-source voltage, where each curve is measured at a fixed gate-source voltage (Fig.1.5).

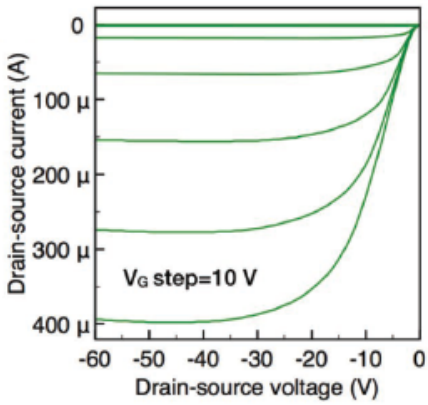

Figure 1.5: An example of an ideal OFET output characteristics [10].

There are different regimes dependently on the V_{DS}: when $V_{DS} < |V_{GS} - V_{TH}|$, the device is found in the linear regime. Here the drain current increases linearly with the V_{DS} and the device acts as a gate voltage controlled variable resistor. At the critical point, where $V_{DS} = |V_{GS} - V_{TH}|$ the area near the drain electrode is depleted of free

charges and the channel becomes pinched off. Finally, when $V_{DS} > |V_{GS} - V_{TH}|$ the increasing potential forces charges from source to drain and the growing depletion zone near the drain causes a saturation of I_{DS}; here the device is in saturation regime.
The transfer characteristic shows the drain current as a function of gate-source voltage with drain-source voltage held constant in the linear or saturation regimes (Fig.1.6).

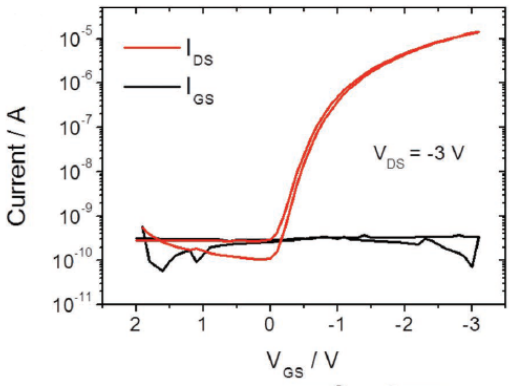

Figure 1.6: An example of a typical transfer characteristics in the saturation regime of a pure TIPS-pentacene OFET [11].

Usually, the transfer characteristic is measured in both directions, gathering data from the highest V_{GS} to the lowest and back to the highest. That is standard procedure because in drive characteristic the forward and backward curves are susceptible to the hysteresis phenomenon, which explains why the two curves do not coincide. Hysteresis combines the transport of carriers, which are induced by the applied bias, and carriers which are released by traps or dielectric relaxation, which can lead to errors in parameter extraction [1] (Fig.1.7).

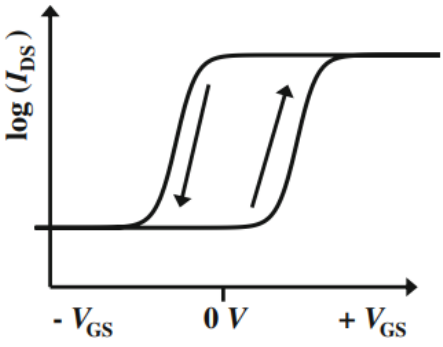

Figure 1.7: A schematic example of the hysteresis phenomenon, observeable on transfer characteristics [12].

The electrical characterization is needed to calculate some parameters which define the transport properties of the device OFET: the mobility μ, the threshold voltage V_{TH}, the ON voltage V_{ON}, the ON/OFF ratio and the subthreshold swing slope S.

Mobility μ is the relationship between the carrier speed in a material and the applied electric field; observed macroscopically, carrier velocity is a viscous flow process in solid materials. The velocity appears constant for a given electric field and is linearly dependent on the field. Mobility is measured in $\frac{cm^2}{Vs}$ and, assuming a linear relationship between carrier velocity and electric field, it is defined by μ= $\frac{Velocity}{E}$. Although, I = QWμE because I is the amount of charge contained in a volume swept at the speed of charge carrier movement, so μ can be expressed as μ= $\frac{I}{QWE}$, where Q is the total charge density and W is the canal width. In organic semiconductors, the relationship is non-linear at larger electric fields and also dependent on the charge carrier concentration; the equation of mobility for organic semiconductors has been approximated to be in saturation

$$\mu = \left(\frac{(\frac{\partial \sqrt{I_{DS}}}{\partial V_{GS}})^2}{\frac{WC_i}{2L}} \right) \tag{1.1}$$

where C_i is the capacitance per unit area of the gate dielectric layer, and L and W are the channel length and width respectively [9].
The threshold voltage is properly the voltage at which occurs the phenomenon of inversion, i.e. the concentration of majoritarian and minoritarian charge carriers reverses. OFETs never achieve inversion and the concept of threshold voltage is meant as the voltage at which the device begins accumulating charges. This indicates the voltage at which there is some increase in current and the device transitions from cut-off to a region of operation in which the device is conducting current.

A simple method for determining the mobility μ and the V_{TH} is to conduct a linear fit on a transfer characteristic curve ($\sqrt{I_{DS}} - V_{GS}$): in the equation of μ (Eq.1.1), $\frac{\partial \sqrt{I_{DS}}}{\partial V_{GS}}$ is the slope of the linear fit, while V_{TH} is the point in which the linear fit intercept the V_{GS} axis (Fig.1.8).

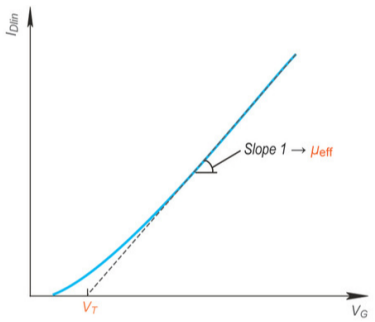

Figure 1.8: A schematic example of mobility and V_{TH} parameters extraction [13].

The ON voltage V_{ON} is the V_{GS} voltage from which the device is operating in an ON state.
The ON/OFF ratio coincides with the fraction of the maximum output current I_{DS} when the device is ON ($V_{GS} > V_{TH}$) over the minimum current, when the device is turned OFF ($V_{GS} < V_{TH}$). It is a phisycal quantity that estimates the field effect efficacy caused by applying a voltage to the gate.
The subthreshold swing slope S represents the velocity of activation of the OFET and it is given by the inverse maximum slope of the saturation transfer characteristic in logarithmic scale $\log I_{DS}$-V_{GS} measured below threshold:

$$S = \frac{\partial V_{\mathrm{GS,min}}}{\partial log I_{\mathrm{D}}}. \tag{1.2}$$

It is typically reported in logarithmic units of $\frac{V}{decade}$. Smaller values of the subthreshold swing slope correspond to a larger slope, which is generally more desirable.

A simple method for determining the V_{ON}, the ON/OFF ratio and the subthreshold swing slope S is to conduct a linear fit on the linear part of a saturation transfer characteristic in logarithmic scale $\log I_D$ vs V_{GS}: V_{ON} corresponds to the voltage at which the curve starts to increase; ON/OFF ratio is the maximum over the minimum current; while S is the inverse maximum slope (Fig.1.9).

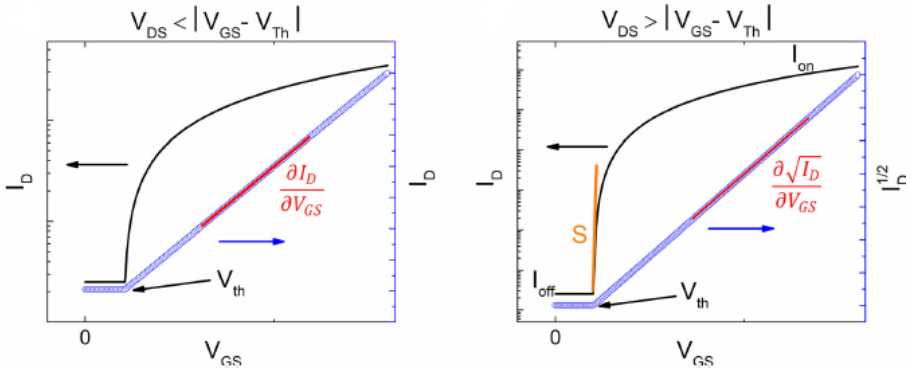

Figure 1.9: ON/OFF ratio and subthreshold swing slope extraction [9].

1.3 Ionizing radiation detectors based on OFETs

Electronic devices such as OFETs, or similar, have proved to be good ionizing radiation detectors; they are sensible to the interaction with the radiation energy that travels in the form of electromagnetic waves (gamma or X-Rays) or particles (protons, electrons). The ionizing radiation detection is becoming crucial in different application fields, ranging from energy, national security, to biological and nuclear research. Inorganic materials

(amorphous silicon, amorphous selenium and diamond) have been intensively explored with this purpose. Even if well performing, the complex growth and fabrication methods needed for large crystalline inorganic detectors often result into high production costs, particularly when large area production is considered; moreover, the typical stiffness of these materials is a limiting factor, especially when device flexibility is required.

When ionizing radiation interacts with the sensitive material constituting the detector, it generates an electric signal which can be measured with appropriate instrumentation. This type of detectors measures the average energy incident on a specific point of the sensitive volume, that is the absorbed radiation dose. Such detectors are known as dosimeters [14]. In the field of radiation detection there are two possible approaches: indirect radiation detection systems, where the radiation is at first absorbed by a scintillating material and then the so obtained visible photons are converted into an electrical signal by a photodetector, and direct detectors, in which the high energy photons are directly converted into an electrical signal [15]. So far, two terminal structure detectors such as photodiodes and photoresistors have been considered. Two terminal organic photodetectors have been mostly used for indirect detection, i.e. integrated with a scintillating material. Only recently, organic materials employment for direct radiation detection has grown in interest. Researches demonstrated that organic flexible detectors can be employed as medical diagnostic (e.g., as bone density analyzer) and dosimetry (e.g., for mammography) tools. Moreover, since their main components are hydrogen and carbon, they are characterized by a low atomic number Z, similar to the average human tissue equivalent Z and this makes them ideal candidates for accurate and reliable real-time in situ dosimetry [16].

Transistor structures have peculiar advantages in the field of radiation detection compared to photodiodes or photoresistors; for instance, transistors are multiparametric devices, where different electrical parameters can be employed for transducing the sensing event. In addition, phototransistors have unique characteristic among electronic devices, such as the possibility of tuning the conductivity by acting on the gate voltage and the intrinsic signal amplification ability, impossible to implement in two terminal structures. Transistor-based sensors are characterized by the ability of being easily integrated in electronic circuits (amplifiers and logic states), providing an easy readout of the signals. All these merits have determined the success of OFET based sensors over two terminal devices in many applications, including biochemical and physical sensing [17].

Many researches and studies analyzed organic devices' response to ionizing radiation exposure. The processes underlying the interaction between organic devices and radiation, especially, have been investigated: the absorbed radiation commonly creates electron-hole pairs that, under the effect of an applied electric field, separate and drift to the respective electrodes, thus generating a photocurrent I_{CC}. In organic semiconductors the observed value of the photocurrent is orders of magnitude higher than the value theoretically calculated which depends on the radiation absorption, showing that there are other processes involved in the generation of such a photocurrent.

In fact, there is an increase in conductivity due to a photoconductive gain, arising when minority charge carriers (i.e. electrons), after being generated by the radiation, are trapped in the organic semiconductor and to maintain charge neutrality majority carriers (holes) are continually being re-injected, which mechanism leads to an amplified photocurrent I_{CC}, with an increase of current ΔI_{PG}:

$$\begin{aligned} \Delta I_{\mathrm{PG}} &= G I_{\mathrm{CC}}, \\ where\ G &= \frac{\tau_{\mathrm{R}}}{\tau_{\mathrm{t}}} \end{aligned} \tag{1.3}$$

is the photoconductive gain, τ_R is a trap recombination time, dependent on the properties of the material and that indicates the characteristic time that electrons remain trapped before recombine, and τ_t is the transit time, it indicates the time in which charge carriers cross the conductive canal, dependent on the device and its mobility [15].

The photocurrent is calculated from the graph reported in Fig.1.10 as the difference between the minimum peaks and the maximum peaks in the I_{DS}.

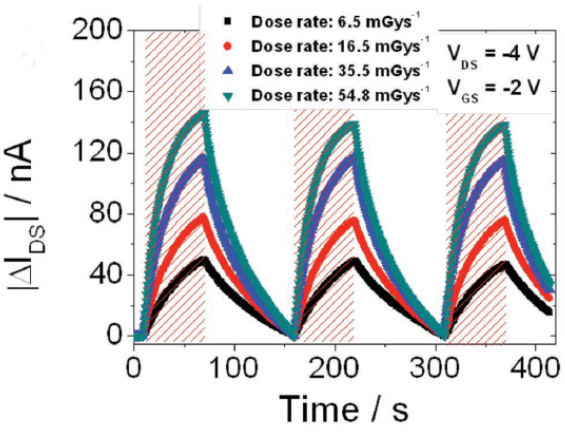

Figure 1.10: An example of a typical dynamical response of the detector to different dose rates of radiation I_{DS} vs t characteristic [17].

Each of these values are then plotted in relation to the Dose Rate, the energy quantity absorbed by a medium, as a result of radiation exposition, per unit of mass, expressed in Gray per seconds $\frac{Gy}{s}$. The curve photocurrent vs dose rate is finally fitted (Fig.1.11) and the slope of the linear fit represents the sensitivity of the detector, expressed in $\frac{\mu C}{Gy}$. Sensitivity is one of the fundamental quantity to evaluate the detection capability of a sensor.

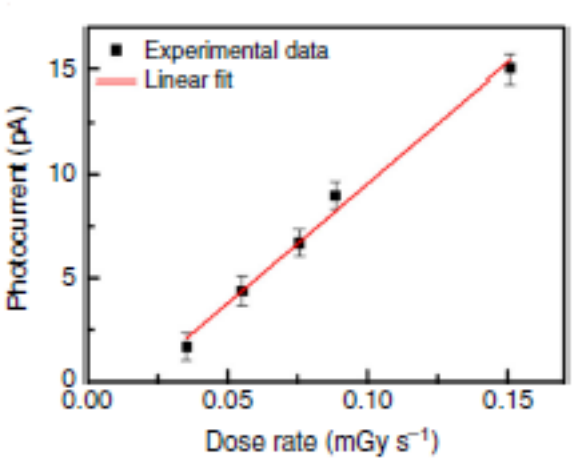

Figure 1.11: An example of a photocurrent vs dose rate graph, including the linear fit used for the sensitivity calculation. [18].

Organic materials, particularly OFETs, are widely used as radiation detectors in medical applications, high-energy physics experiments, plant laboratories, airport security and radiation sensing for nuclear installation. Especially in the medical field there is a growing interest in the development of devices suitable for ionizing radiation detection such as OFETs, especially because OFETs are lightweight, conformal to the curvature of the human skin surface and thin enough to be placed at the site of irradiation without disturbing the delivered dose. The similarity in the density of organic compounds and human tissue, given by the comparable atomic numbers (Z), minimizes the correction factor for estimating the dose applied to the patient [19]. Furthermore, commercially available personal dosimeters are rigid and uncomfortable to be worn or used for the examination of an organ, while organic semiconductors are flexible and wearable. They are easily processable and deposited in liquid phase by low-cost techniques at low temperature onto flexible and conformable substrates and even synthetic and natural textiles, therefore particularly convenient for wearable electronics [16].

1.4 Radiation Hardness

One of the most interesting feasible study on ionizing radiation sensors is radiation hardness; that is the process of making electronic components and circuits resistant to damage or malfunction caused by high levels of ionizing radiation. The evaluation of significant changes of device performance because of damages in the materials related to the X-Ray exposure is fundamental to define the reliability of the detector. Devices' ability to withstand increasing amount of radiation is tested by increasing the total dose

of exposure, in different stress conditions. Total dose testing is performed by exposing a device to an ionizing radiation environment and by measuring its electrical and sensing performances for a variety of operating conditions. This is achieved by step-stress testing, performed by first characterizing the electrical performances of the device, exposing it to a fixed dose of ionizing radiation, and then measuring again the electrical parameters to determine their change. To determine the device response versus total dose, the test is performed with different samples of the same type at several accumulated dose levels. The step stress approach is usually more convenient and much more widely used [20]. A high total dose of radiation causes slow gradual degradation of the device's performance and, for OFETs, it can be measured collecting transfer characteristics in the saturation region before and after each cycle. From each characteristic, device parameters can be extrapolated and converted into percentual to correlate them to the total dose. Every parameter shows how the OFET performance is afflicted by the X-Ray irradiation.

Many fields require devices which are capable of maintain an high endurance to radiation: in the medical field, dosimeters can be used to examine tumorous organs; in the military and space industry, radiation-hardened and radiation tolerant components are often used for satellite system power supplies, to step down switching regulators, microprocessors and high efficiency, low voltage subsystem power supplies; in telecommunication, nuclear hardness is in great demand because the physical attributes of an electronic component will allow survival in an environment that includes nuclear radiation and electromagnetic pulses. Bipolar devices radiation response often depend strongly on dose rate, energy, and bias during irradiation, and one rarely is able to test a device in the laboratory in exactly the radiation environment that the part is required to withstand. So, correlation between laboratory to use environments is required [21].

A few examples of tests used for measuring the radiation hardness of electrical devices are reported afterwards for some of the most significant fields.

Many conventional bipolar linear microcircuits used in space systems have shown a dose rate sensitivity to total dose degradation. Dose rate data are presented in terms of sensitive parameter shifts at a fixed dose and dose rate enhancements factors. These investigations have found that many of the conventional bipolar linear circuits used in spacecraft show enhanced degradation at dose rates below the dose rate range of 50-300 rad, which corresponds to 0.5-3 Gy. In most cases bipolar linear microcircuits exhibit significant parameter degradation before functional failure. Therefore the total dose data are presented in terms of the change in a sensitive parameter from the preirradiation value. The change is shown for a dose where the sensitive parameter either starts to degrade significantly or exceeds the preirradiation specification value (or, in some cases, at the highest dose level tested). Recent data on the dose rate response of bipolar linear circuits have been presented in the form of a summary of the change in the most sensitive parameter at 50 krads, equal to 500 Gy, the change in the parameter at a dose where significant changes occur and the enhancement factor at the lower dose rates [22].

To assure the radiation hardness of microelectronic devices, the radiation effect community developed the radiation hardness test guidelines as MIL-STD-883, Method 1019, JESD57, and ASTM F1192 (Schwank, 2008). Radiation hardness assurance test methods are used to define tests which will provide significant insight into electronic device behavior in radiation environments. Ionizing radiation test procedure, specified in method 1019 of MIL-STD-883, defines requirements for total dose radiation effects from a cobalt-60 gamma ray source (Spour, 1988). This test is performed in two phases. The first phase of the test is intended to determine parametric or functional failure of an electronic device. Large shifts in threshold voltage, initiated by positive charge trapped in the microelectronic devices, will cause current leakage. This phase of the test requires irradiation at room temperature with a dose rate between 50 and 300 rads(Si)/s (0.5-3 Gy/s) until specified dose rate will be reached. Electrical measurements are required before and after the irradiation process using the same measurement system and sequence (MIL-STD-883, 2010). The second phase requires irradiation of specimens up to 50% of the specified dose, followed by the annealing at 100°C for 168 hours under worst-case conditions. The second phase is used to define worst-case bias conditions [23].

Chapter 2

Materials and Methods

2.1 Devices under Test

In this thesis it is reported the full characterization of two samples, which are two thin film devices composed of four OFETs each, arranged in a 2x2 matrix as depicted in Fig.2.1, where D, S and G stand for drain, source and gate electrodes numbered by the corresponding OFET position.

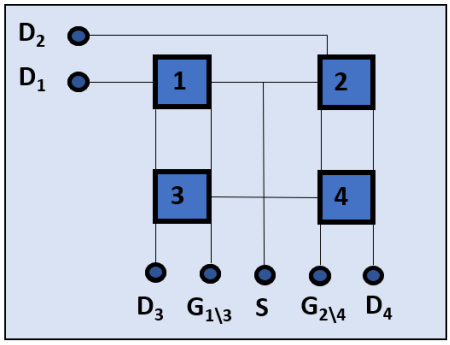

Figure 2.1: A sketch of the sample structure with four OFETs (1, 2, 3, 4) and their respective electrodes of drain D, source S, gate G.

The devices geometric structure used is the bottom gate bottom contacts one: OFETs' fabrication took place in the University of Napoli while I carried on the deposition of the organic semiconducting layer here at the University of Bologna. The gate terminal has been made of aluminum, while the source and drain terminals have been made of gold with interdigitated structures. They have been deposited by thermal evaporation and patterned by photolithography. Interdigitated structures are means to achieve a greater conductive canal width keeping a limited pixel area. They consist in shaping the electrodes into toothed structures, where the conductive canal lenght L is the distance

between two teeth, while the width W is given by the entire path between the teeth (Fig.2.2).

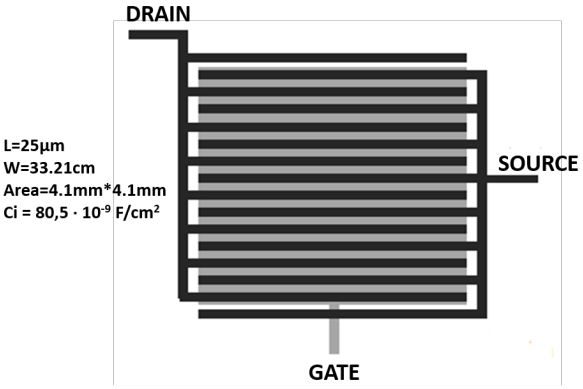

Figure 2.2: A schematic representation of interdigitated structures used for increasing the conductive canal width; L is the canal lenght, given by the distance between two teeth; also the conductive canal parameters values are reported.

The dielectric layer has been made of aluminum oxide Al_2O_3 and it is 100nm thick. The deposition method of the dielectric layer is different depending on the samples: in one case it has been fabricated by depositing the first 30nm through aluminum anodizing and the last 70nm through thermal evaporation, while in the other case it has been deposited only through evaporation. The OFETs structure is shown in Fig.2.3, where the substrate is made by PEN (polyethylene naphthalate), a material that combines flexibility and resistance.

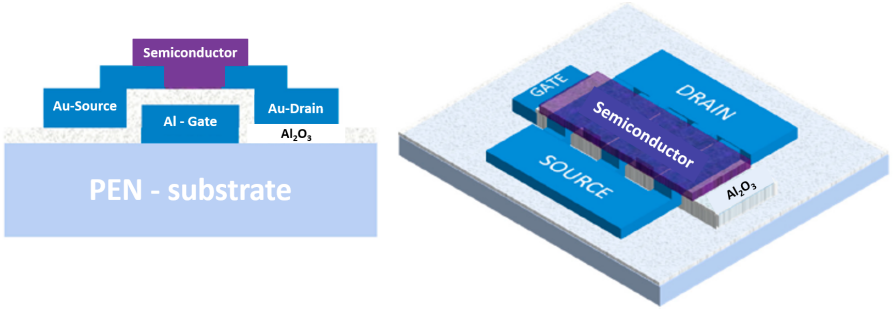

Figure 2.3: The analyzed OFETs structure [24].

The organic semiconductor, on the contrary, has been deposited here at the University of Bologna as last step. Two different organic semiconducting small molecules have been deposited by means, 6,13-Bis(triisopropylsilylethynyl)pentacene (TIPGe-pentacene and

TIPS-pentacene) (Fig.2.4) by drop-casting technique (Fig.2.5). Both solutions were at 0.5% in toluene with 0.00087 g mass in 200 µL of solution.

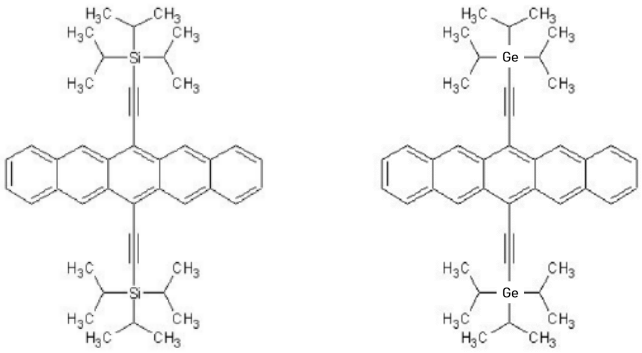

(a) TIPS-pentacene **(b)** TIPGe-pentacene

Figure 2.4: TIPS and TIPGe-pentacene molecules.

After the deposition, the samples have been annealed through a M2-A ARGOlab hot plate for one hour at about 90°C to let the solvent completely evaporate and the organic molecules crystallize forming a polycrystalline thin film (Fig.2.5).

(a) Pipette **(b)** M2-A ARGOlab

Figure 2.5: (a) The pipette used for depositing the semiconductor layer through drop-casting technique. (b) The M2-A ARGOlab hot plate used for the annealing of the samples after the semiconductor layer deposition.

2.2 Data collection and analysis

After the organic semiconductor deposition, the two samples have been electrically characterized. Electrical characterization consists into acquiring the characteristics curves

of the transistor discussed in the previous chapter, working on different region. In order to collect these data, the examined OFET has been put into a Faraday cage and through an optical microscope and three conductive tips moved by micro-manipulators have been connected to three terminals: the source electrode has been connected to ground, the gate and drain electrodes respectively to the channel 1 and channel 2 of a SMU Keithley 2614B source meter (Fig.2.6).

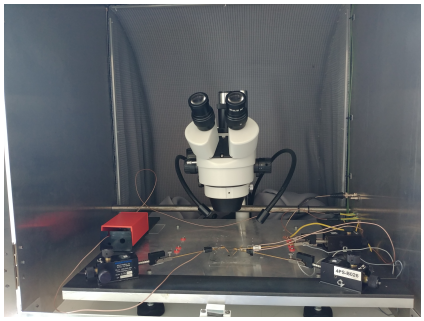

(a) Optical microscope and manipulators inside a Faraday cage

(b) SMU Keithley 2614B source meter

VOLTAGE ACCURACY SPECIFICATIONS

Range	Source			Measure	
	Programming resolution	Accuracy ± (% reading + volts)	Typical noise (peak to peak) 0.1 Hz to 10 Hz	Display resolution	Accuracy[4] ± (% reading + volts)
200 mV	5 µV	0.02% + 375 µV	20 µV	100 nV	0.015% + 225 µV
2 V	50 µV	0.02% + 600 µV	50 µV	1 µV	0.02% + 350 µV
20 V	500 µV	0.02% + 5 mV	300 µV	10 µV	0.015% + 5 mV
200 V	5 mV	0.02% + 50 mV	2 mV	100 µV	0.015% + 50 mV

CURRENT ACCURACY SPECIFICATIONS

Range	Source			Measure	
	Programming resolution	Accuracy ± (% reading + amperes)	Typical noise (peak to peak) 0.1 Hz to 10 Hz	Display resolution	Accuracy[4] ± (% reading + amperes)
100 nA	2 pA	0.06% + 100 pA	5 pA	100 fA	0.06% + 100 pA
1 µA	20 pA	0.03% + 800 pA	25 pA	1 pA	0.025% + 500 pA
10 µA	200 pA	0.03% + 5 nA	60 pA	10 pA	0.025% + 1.5 nA
100 µA	2 nA	0.03% + 60 nA	3 nA	100 pA	0.02% + 25 nA
1 mA	20 nA	0.03% + 300 nA	6 nA	1 nA	0.02% + 200 nA
10 mA	200 nA	0.03% + 6 µA	200 nA	10 nA	0.02% + 2.5 µA
100 mA	2 µA	0.03% + 30 µA	600 nA	100 nA	0.02% + 20 µA
1 A	20 µA	0.05% + 1.8 mA	70 µA	1 µA	0.03% + 1.5 mA
1.5 A	50 µA	0.06% + 4 mA	150 µA	1 µA	0.05% + 3.5 mA
10 A[6]	200 µA	0.5% + 40 mA	N/A	10 µA	0.4% + 25 mA

(c) SMU Keithley 2614B specifications

Figure 2.6: (a) The optical microscope and the manipulators used for connecting the source, drain and gate elctrodes to the source meter terminals. (b) The SMU Keithley 2614B source meter used for the electrical characterization on the samples. (c) The SMU Keithley 2614B source meter specifications.

The source meter experimental setup has been set with initial delay at 100ms, delay per step at 100ms and aperture time at 50ms. Through a custom acquisition software, each OFET of each sample has been characterized by acquiring the output, the transfer characteristics in saturation regime and in linear regime. To do so, the values of V_{GS} and V_{DS} have been set as:

- Output characteristic I_D/V_{DS}: V_{DS} varies from 0 to -3V with a 0.2V step, V_{GS} varies from 1 to -3V with a 1V step;
- Transfer characteristic in saturation region I_D/V_{GS}: V_{GS} varies from 1 to -3V with a 0.2V step, V_{DS} =-3V;
- Transfer characteristic in linear region I_D/V_{GS}: V_{GS} varies from 1 to -3V with a 0.2V step, V_{DS} =-0.2V.

For the output characteristic only the forward curve of I_D vs V_{DS} has been plotted; for the transfer characteristic in saturation region the square root of I_D vs V_{GS} and in linear region the absolute value of I_D vs V_{GS} have been plotted. On the saturation transfer characteristic, the most linear part has been selected and fitted. From the linear fit, the values of mobility and threshold voltage have been extracted: the threshold voltage corresponds to the point in which the linear fit intercepts the x axis, while mobility follows the 1.1, in which $(\frac{\partial\sqrt{ID}}{\partial V_{GS}})^2$ is equivalent to the slope obtained through the linear fit. On the logarithmic transfer characteristic, the values of V_{ON}, ON/OFF ratio and subthreshold swing slope S have been extracted; only the forward curve has been graphed on logarithmic scale. The ON voltage corresponds to the point in which the curve starts to rapidly increase; the ON/OFF ratio is given by the maximum current over the minimum; the subthreshold swing slope S is the inverse of the maximum slope and it is measured in $\frac{V}{dec}$.

The analysis continued with the characterization through ionizing radiation: the two samples have been irradiated with an X-Ray beam and their response has been monitored. X-Ray characterization is typical of ionization radiation detectors such as OFETs; what matters is to acquire a pristine saturation transfer before the irradiation, an after X-Ray saturation transfer after the exposition to X-Rays and the characteristic of the drain current over time during the exposure for various cycles of measures. In order to achieve that, the samples have been enclosed in a Faraday cage and electrically connected to a SMU Keithley 2614B source meter. The Faraday cage has been locked, so that light could not interact with the sample on the inside during the X-Ray exposure; then centered and positioned at 29 cm of distance from the X-Ray source emitted by a molybdenum tube as depicted in Fig.2.7a.

The X-Ray tube is an instrument able to convert the kinetic energy of accelerated electrons by a strong electric field into electromagnetic radiation. Inside the tube, where the vacuum has been established, a high voltage is applied between anode and a filament

which acts as cathode. The filament is heated through Joule effect and it starts emitting electrons by thermionic effect, which, accelerated by the potential difference, collide on the anode. The characteristic radiation is produced by electrons collision on anode atoms. When an anode electron is ejected from his energy level, an electron from an upper shell replaces it, emitting a photon with energy equal to the difference between the two energy levels. Because of the electrical interaction between anode atoms, electrons are highly decelerated and the kinetic energy variation is converted into electromagnetic radiation, leading to the braking radiation (Brehmmstrahlung Fig.2.7a). The X-Ray tube used for irradiating the samples is a PANalytical PW2285/20 with a molybdenum target. To realize different radiation dose rates the tube voltage has been kept at 40 kV and the filament current has been varied from 10 to 50 mA (Fig. 2.7 b and c).

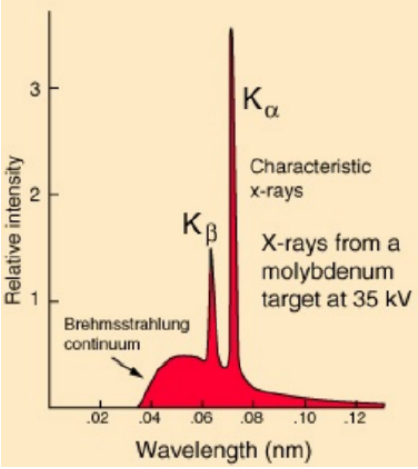

(a) Typical X-Ray tube emission spectrum

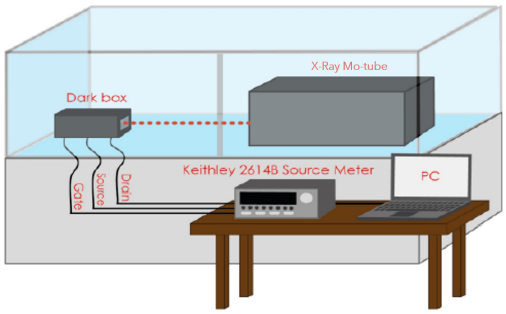

(b) Scheme of the instrumental setup

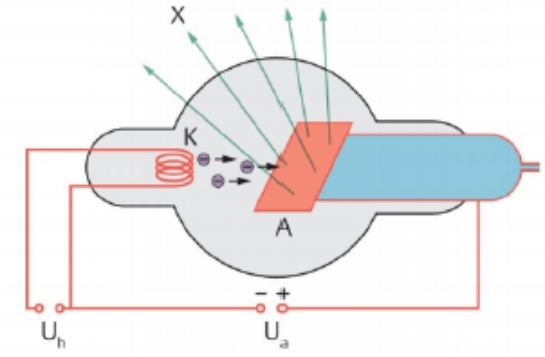

(c) Scheme of the X-Ray tube

Figure 2.7: (a) A typical emission spectrum of an X-Ray tube. (b) The instrumental setup used for the X-Ray irradiation of the samples. (c) The schematic of a X-ray tube.

Through a shutter connected to a timer it has been possible to alternate periods of darkness to periods of x-ray exposure. 60 seconds intervals have been chosen in order to have fairly high discharge times maintaining the operating conditions typical of most relevant applications.

Through a custom program written in LabVIEW environment, many types of data have been acquired: transfer characteristics in saturation region before (pristine) and after X-Ray exposition (after XR); the drain current characteristic I_D/t during the X-Ray dose rates for different cycles of measures, dictated by the filament current; and the sensitivity curve photocurrent vs dose rate. In order to do that, the following values have been set:

- Transfer characteristic in saturation region I_D/V_{GS}: V_{GS} varies from 1 to -3V with a 0.1V step, V_{DS} =-3V;
- Radiation exposition curve I_D/t: V_{DS} =-3V, V_{GS} =-2V, t_{ON}=60s, t_{OFF}=60s, Dose Rates = 12.0, 24.3, 36.6, 48.9, 61.3 $\frac{mGy}{s}$.
- Sensitivity curve Photocurrent/Dose Rate: the photocurrent has been calculated by subtracting the minimum peaks to the maximum in the I_D/t curve. The sensitivity is the slope of the linear fit performed on this graph; it is expressed in $\frac{mA}{\frac{mGy}{s}}$, i.e. $\frac{\mu C}{Gy}$.

The drain current characteristic I_D/t during the X-Ray exposition has been plotted and normalized for each value of the filament current. Finally, photocurrent values have been calculated and a linear fit has been performed on the photocurrent vs dose rate graph.

The collected data of I_D vs time characteristic have been manipulated and elaborated: for each filament current of each transistor, a second degree polynomial fit has been executed on the minimum current value (dark current) for each cycle (three points) and then subtract from the original values of I_D current. Thus, the possible drift of the current trend has been removed and the characteristic normalized (Fig.2.8 a and c). An example of the polynomial fit executed is shown in Fig. 2.8b.

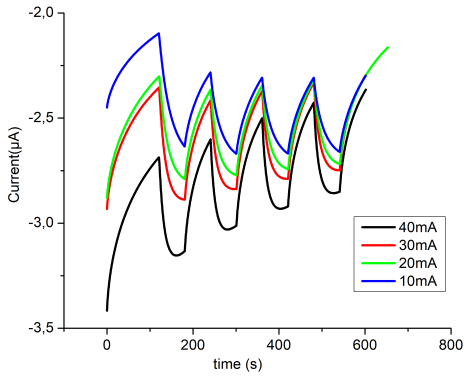

(a) Graph pre-normalization

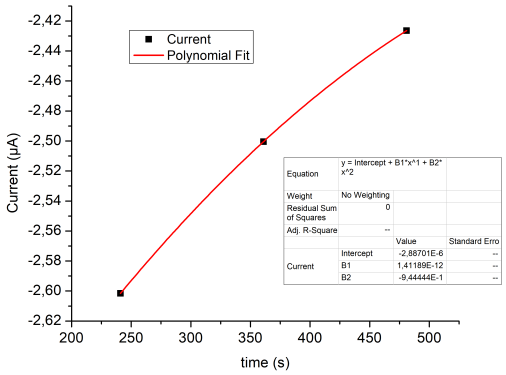

(b) Polynomial fit

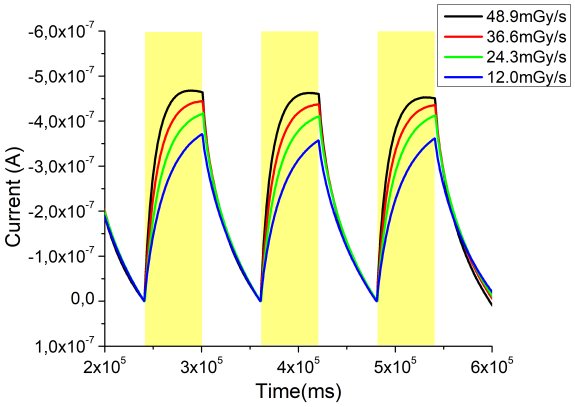

(c) Graph post-normalization

Figure 2.8: (a) The graph before normalization. (b) The polynomial fit executed to normalize the photocurrent curve. (c) The same graph after normalization.

A linear fit on each sample's photocurrents has been performed as a function of dose rate: the slope of the resulting line is the sensitivity of the examined transistor. In Fig. 2.9 an example of the linear fit of the photocurrent is shown as function of the dose rate.

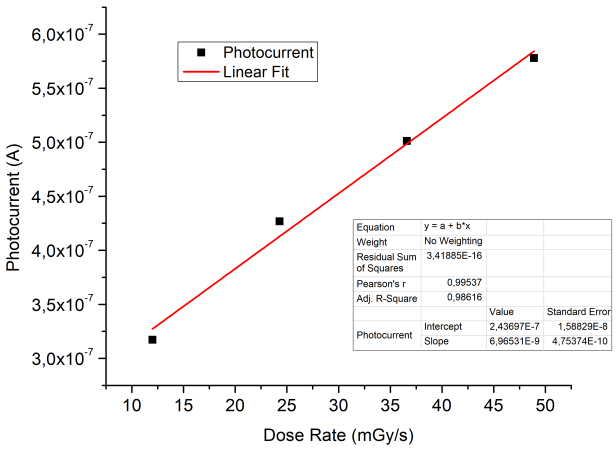

Figure 2.9: The weighted linear fit on photocurrent as dose rate's function to determine the sensitivity.

On a TIPS based OFET a radiation hardness study has been conducted to analyze how the sample performance changes dependently on the irradiated quantity of total dose, using the same experimental setup. The X-Ray charcterization took place on the March 22nd 2021, while the radiation hardness study on the March 24th 2021 after 42 hours of storage in dark. The pristine characteristic referred to afterwards is the one acquired before the X-Ray characterization on the March 22nd. The followed procedure for the radiation hardness study is: firstly, a pristine saturation transfer is acquired; secondly, the sample has been irradiated for four I_D/t peaks at a set Dose Rate (61.3 $\frac{mGy}{s}$), composed of 60 seconds of exposition to radiation (t_{ON}) and 60 seconds at rest (t_{OFF}); finally, an after radiation saturation transfer is acquired. This procedure is repeated for seven times and, because of the tube voltage set at 40kV and the filament current set at 50mA, the total dose detected by the sample increases of 50 units for each cycle, reaching the value of 300Gy. The calculus of the total dose is extracted by the calibration of the Mo-tube, as shown in Tab.2.1.

Tube Current (mA)	**Dose Rate ($mGys^{-1}$)**
10	12.0
20	24.3
30	36.6
40	48.9
50	61.3

Table 2.1: Mo-X-Ray tube calibration, effectuated on the 28^{th} January 2021.

A graph in which saturation transfer characteristics are confronted has been plotted for every partial total dose (Pristine, 50, 100, 150, 200, 250, 300 Gy) both on logarithmic and linear scale. The parameters of mobility, threshold voltage and photocurrent have been calculated through the methods previously showed. They have been reported compared to their initial value and plotted in a variation (%) vs total dose (Gy) graph, showing visually the performance loss of the examined sample. Finally, the drain current curve I_D/t has been plotted, showing the photocurrent peaks after every exposition to radiation.

Chapter 3

Results and discussion

3.1 Electrical response

All examined OFETs have reproduced well the expected trend for each characteristic; this similarity is evident when confronted with previous literature for similar devices [17]. The output, the saturation transfer on both logarithmic and linear scale and the linear transfer on both logarithmic and linear scale characteristics are reported in Fig.3.1 and in Fig. 3.2 for both a TIPGe-Pn based OFET and a TIPS-Pn based OFET respectively.

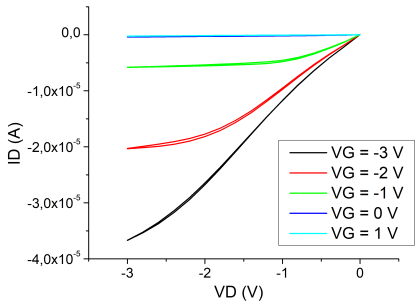

(a) Output characteristic

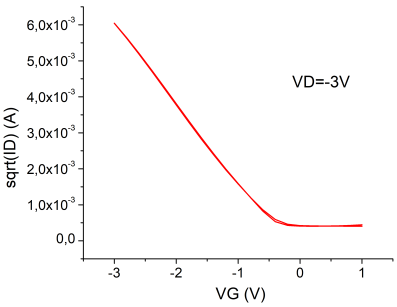

(b) Transfer characteristic in saturation region

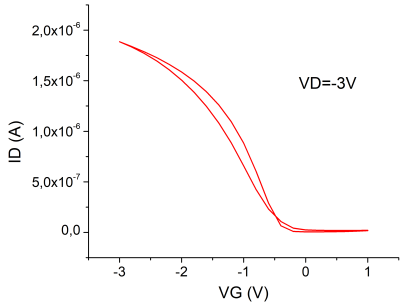

(c) Transfer characteristic in linear region

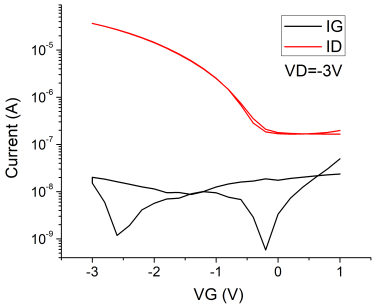

(d) Transfer characteristic in saturation region on a logarithmic scale

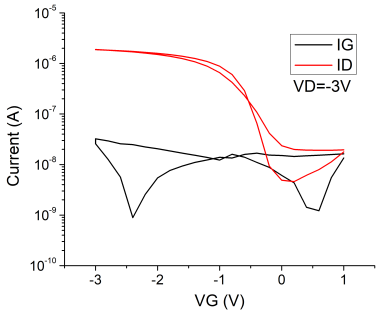

(e) Transfer characteristic in linear region on a logarithmic scale

Figure 3.1: For TIPGe-Pn based OFET4 (a) The output characteristic, showing the different values of V_{GS}. (b) The transfer characteristic in saturation region (VD=-3V). (c) The transfer characteristic in linear region (VD=-3V). (d) The transfer characteristic in saturation region, showing the different curves of I_G and I_D, on a logarithmic scale. (e) The transfer characteristic in linear region, showing the different curves of I_G and I_D, on a logarithmic scale.

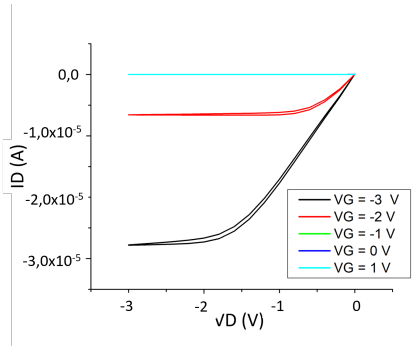

(a) Output characteristic

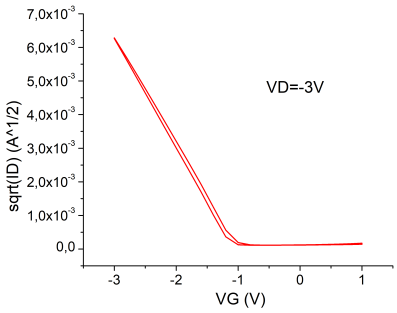

(b) Transfer characteristic in saturation region

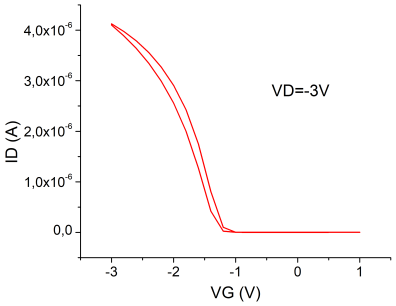

(c) Transfer characteristic in linear region

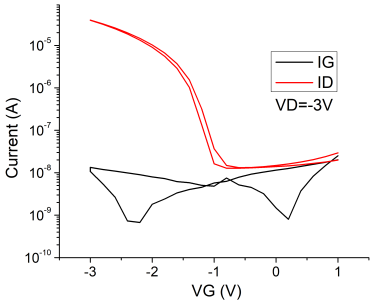

(d) Transfer characteristic in saturation region on a logarithmic scale

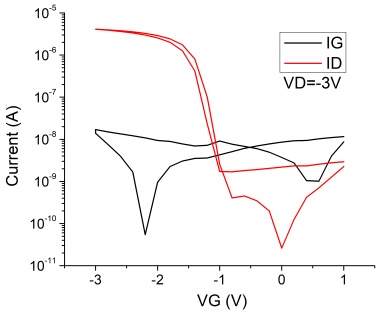

(e) Transfer characteristic in linear region on a logarithmic scale

Figure 3.2: For TIPS-Pn based OFET1 (a) The output characteristic, showing the different values of V_{GS}. (b) The transfer characteristic in saturation region (VD=-3V). (c) The transfer characteristic in linear region (VD=-3V). (d) The transfer characteristic in saturation region, showing the different curves of I_G and I_D, on a logarithmic scale. (e) The transfer characteristic in linear region, showing the different curves of I_G and I_D, on a logarithmic scale.

The curves show a good agreement with the expected trend [17], which is validated by the comparison between the extracted parameters and the literature ones, as explained afterwards. The comparison between transfer characteristics in saturation region is shown in Fig.3.3. All OFETs of the same sample are nominally equal, which implies the uniformity of all electrical characteristics. If compared, it can be seen that the electrical characteristics are not nominally equal, but there is a good resemblance, especially for the TIPS-Pn based device. The main discrepancies in the electrical responses between the OFETs of a same device could be given by the accidental differences performed during the process of fabrication or by accidental damages caused to the material. OFETs are particularly sensitive to external environments (light, temperature, etc) and to incidental pressures or incisions performed during the characterization process, which explains the possible damages occurred to the samples.

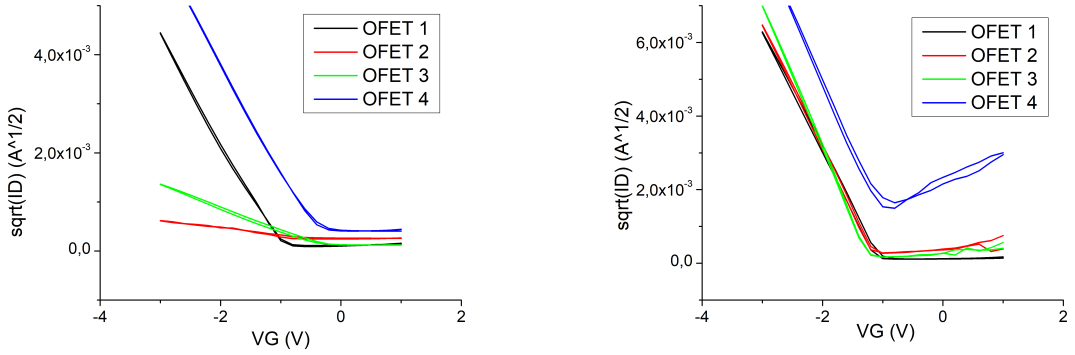

(a) TIPGe-Pn based

(b) TIPS-Pn based

Figure 3.3: (a) The comparison between the transfer characteristics of TIPGe-Pn based. (b) The comparison between the transfer characteristics of TIPS-Pn based.

Furthermore, the TIPS-based electrical parameters extrapolated from the characteristics validate their correspondence with data reported in literature for analogous devices (μ= 0.1 cm^2/Vs, V_{TH} = 0.4 V [17]). On the contrary, the sample TIPGe-based showed poorer electrical performances if compared with the ones reported in the past research (μ= 0.4 cm^2/Vs [25]).

In Tab.3.1 the mobility, threshold voltage, V_{ON}, ON/OFF ratio and subthreshold swing slope S values are reported with the respective uncertainty for each sample. The values reported in the table have been avaraged over several OFETs nominally identical both for the TIPS-based and for the TIPGe-based sample. The parameters calculated are comparable to those of previous studies: mobility 0.28 $\frac{cm^2}{Vs}$, threshold voltage -0.2 V, ON/OFF ratio 10^2-10^5 [25].

SAMPLES	Mobility μ ($\frac{cm^2}{Vs}$)	V_{TH} (V)	V_{ON} (V)	ON/OFF	S ($\frac{V}{decade}$)
TIPGe-based	(9.3±0.5)·10^{-3}	-0.7±0.5	-0.5±0.4	1300±1500	0.4±0.2
TIPS-based	(2.2±0.5)·10^{-2}	-1.1±0.1	-0.9±0.1	1700±1200	0.25±0.01

Table 3.1: Parameters calculated through electrical characterization.

Mobility, threshold voltage, V_{ON} and ON/OFF ratio uncertainties have been determined through the standard deviation formula, as shown in Appendix A, while the linear fit operated on the transfer characteristics gives the uncertainties on the subthreshold swing slope.

3.2 X-Ray detection

The TIPS-based device, particularly, has proved itself to be a good ionizing radiation detector: its characteristics fully reflect the expected trends of previous studies [17]. In Fig.3.4 the trend of the drain current of the first OFET can be seen for three cycles of irradiation, for several dose rates of irradiation; the graph shows how the response to ionizing radiation is perfectly clear and evident. In fact, the yellow area shows the time intervals in which the device has been irradiated, while in the other regions the device has been kept in dark. Each highlighted area corresponds to a time interval of t_{ON}=60s and the dark regions to a time interval t_{OFF}=60s.

To evaluate the sensing capability of each OFET to the ionizing radiation, the sensitivity has been extrapolated from the linear fit of the curve reported in Fig.2.9. In Tab.3.2 the sensitivity values normalized on the pixel area (A=16.81 mm^2) are reported for each sample with the linear fit errors used as uncertainties.

SENSITIVITY ($\frac{\mu C}{Gycm^2}$)	OFET 1	OFET 2	OFET 3	OFET 4
TIPGe-Pn based	13±2	/	0.45±0.06	/
TIPS-Pn based	15±2	32±3	19±3	41±3

Table 3.2: Sensitivity values calculated for each sample OFET through X-Ray radiation exposition.

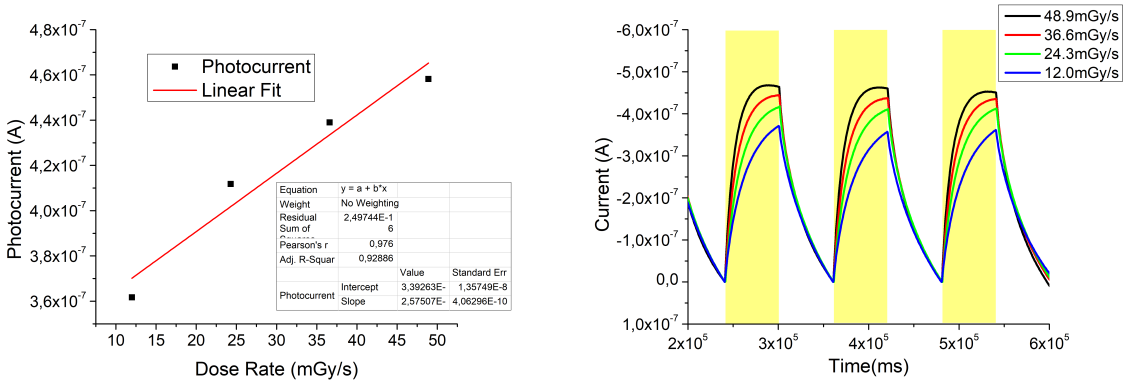

(a) Photocurrent vs Dose Rate graph and linear fit

(b) I_D vs time characteristic

Figure 3.4: For the TIPS-Pn based OFET 1: (a) Photocurrent vs Dose Rate graph from which sensitivity has been extracted through a linear fit. (b) The characteristic curve I_D vs time, for three cycles of X-Ray exposition, each one on 60 seconds of irradiation (t_{ON}) and 60 seconds in dark (t_{OFF}); the yellow area points out the time interval in which the device is irradiated.

These values validate the thesis that OFETs are good ionizing radiation detectors: either TIPGe-Pn based OFET 1 or all of TIPS-Pn based OFETs have sensitivity values that are comparable with the values reported in the past for similar polarization conditions: 1200 $\frac{nC}{Gy}$, which corresponds to 7.14 $\frac{\mu C}{Gycm^2}$ [17]; 4460 $\frac{nC}{Gy}$, which corresponds to 26.5 $\frac{\mu C}{Gycm^2}$ [25]; 200 $\frac{nC}{Gy}$, which corresponds to 1.2 $\frac{\mu C}{Gycm^2}$ [15]. Only TIPGe-Pn OFET 3 sensitivity does not show a good agreement, but that is because OFETs are sensitive to the contact with the surrounding environment (light, temperature, etc) and to non intentional pressures during the characterization.

In Tab.3.3 the parameters calculated through the radiation hardness study are reported in correspondence of each partial total dose absorbed by the detector, each with the relative error (Appendix A).

Total Dose (Gy)	Mobility μ ($\frac{cm^2}{Vs}$)	V_{TH} (V)	V_{ON} (V)
0	$(2.3\pm0.1)\cdot10^{-2}$	-1.35±0.01	-1.0±0.3
50	$(1.9\pm0.1)\cdot10^{-2}$	-1.31±0.01	-0.7±0.3
100	$(1.9\pm0.1)\cdot10^{-2}$	-1.33±0.01	-0.7±0.3
150	$(2.0\pm0.1)\cdot10^{-2}$	-1.31±0.01	-0.4±0.3
200	$(2.1\pm0.1)\cdot10^{-2}$	-1.33±0.01	-0.4±0.3
250	$(2.1\pm0.1)\cdot10^{-2}$	-1.34±0.01	-0.4±0.3
300	$(2.1\pm0.1)\cdot10^{-2}$	-1.34±0.01	-0.3±0.3

Total Dose (Gy)	ON/OFF	S ($\frac{V}{decade}$)	Photocurrent (A)
0	800±300	0.32±0.08	$(10\pm1)\cdot10^{-7}$
50	1900±300	0.38±0.08	$(5.7\pm0,3)\cdot10^{-7}$
100	1700±300	0.45±0.08	$(4.8\pm0,3)\cdot10^{-7}$
150	1500±300	0.53±0.08	$(4.6\pm0,4)\cdot10^{-7}$
200	1400±300	0.51±0.08	$(5.0\pm0,9)\cdot10^{-7}$
250	1300±300	0.53±0.08	$(3.8\pm0,2)\cdot10^{-7}$
300	1300±300	0.53±0.08	$(4.3\pm0,4)\cdot10^{-7}$

Table 3.3: Parameters calculated through the radiation hardness study for TIPS-Pn based OFET 2.

The radiation hardness study has resulted into a good performance of the sample; even though mobility, threshold voltage and photocurrent have lost a low percentage of performance during the first cycles of irradiation, the OFET has not suffered long term damages. A graph variation reported as a function of total dose has been plotted to show how each parameter varies during the X-Ray exposure. The radiation hardness test has been executed for total dose rising up until the highest value of 300 Gy, which is particularly high if compared with previous radiation hardness studies (for example, a total dose of 160Gy [17]). This value of total dose falls within the testing range of the radiation hardness test guidelines cited in the first chapter, which reaches total dose of 500 Gy [22]-[23]. As it can be seen in the graph variation vs total dose (Fig.3.5), the device exposure to such a quantity of total dose has not damaged its electrical response nor its detecting capacity. In fact, its trend shows a correct electrical and detecting behavior, proving that the high total dose exposure does not preclude its use.

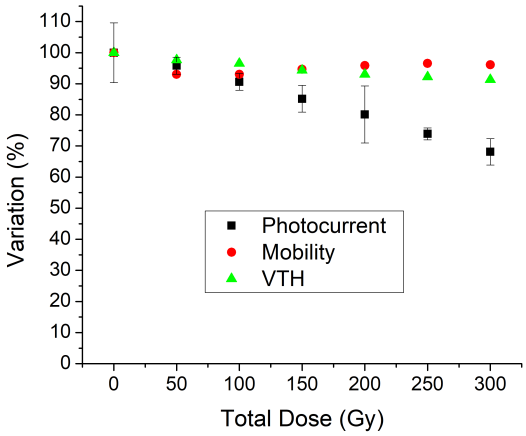

Figure 3.5: TIPS-based OFET 2 mobility, threshold voltage and photocurrent variation as total dose function.

Finally, it is reported the comparison between the transfer characteristics both on linear and logarithmic scale before and after 44 Gy of X-Ray exposure and the same curve acquired after 42 hour of storage in dark (Fig.3.6). These graphs show a stable electrical behaviour of the OFET after the 44 Gy of irradiation.

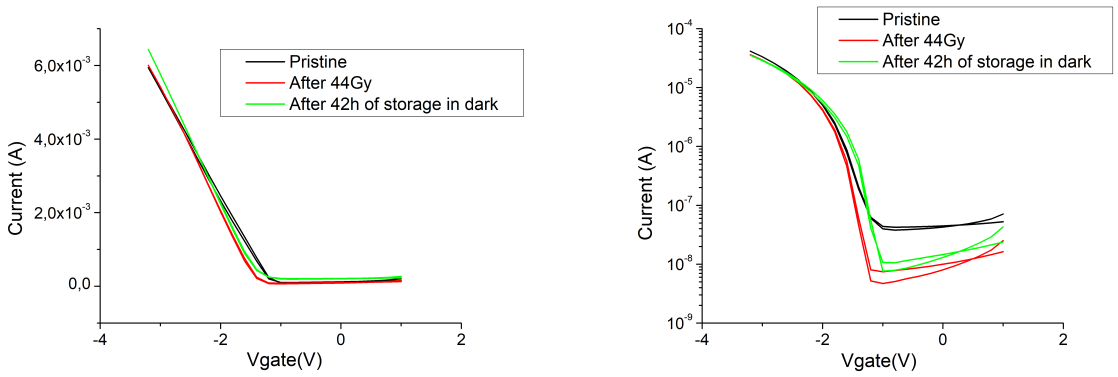

(a) Saturation transfer characteristics on a linear scale

(b) Saturation transfer characteristics on a logarithmic scale

Figure 3.6: (a) The comparison between the transfer characteristics of TIPS-based on a linear scale. (b) The comparison between the transfer characteristics of TIPS-based on a logarithmic scale.

Conclusions

Different organic field effect transistors have been fabricated, characterized and a radiation hardness study has been conducted, in order to test their tolerance to ionizing radiation. The organic semiconductor deposited by drop-casting technique on each sample is a small molecule solution, respectively of TIPGe- and TIPS-pentacene, in toluene solvent. The target of this study was to test these two samples radiation tolerance, in order to investigate their X-ray detection properties and whether they could be good ionizing radiation dosimeters. Most importantly, the fundamental parameters that distinguish transistors (mobility, threshold voltage V_{TH}, ON voltage V_{ON}, ON/OFF ratio, subthreshold swing slope S) and their photocurrent and sensitivity to X-Ray have been calculated, from collected data, and graphed for each sample. Thus, it has been determined that the difference in the fabrication technique of the two samples generate different performances. Results can be summarized as follows:

- Examined transistors show good output characteristics, which indicates their ability to vary their performances dependently on the gate voltage. TIPS-Pn based sample responded better to electrical characterization, its parameters values, especially mobility μ= (0.023±0.005) $\frac{cm^2}{Vs}$, are comparable with those reported in previous studies: in L. Basiricò, Nat Comm 2016 [15], it is reported a mobility value of μ= 0.02 $\frac{cm^2}{Vs}$. TIPGe-Pn based sample, instead, has not showed a good electrical response as the ones in the past research: mobility μ= (0.0093±0.0005) $\frac{cm^2}{Vs}$ is not comparable with the value reported in A. Ciavatti, Adv. Func. Mat. 2018 [25] of mobility 0.28 $\frac{cm^2}{Vs}$. On the contrary, the values of threshold voltage and ON/OFF ratio of both devices are comparable to those of the same research: threshold voltage -0.2 V, ON/OFF ratio 10^2-10^5 [25].

- The X-Ray characterization has given good I_D vs time characteristics and good values of sensitivity for both devices, comparable with the ones reported in previous studies for similar polarization conditions [17]. The sensitivity target was of about 20 $\frac{\mu C}{Gycm^2}$, which falls within the confidence interval of the calculated values.

- For what concerns the radiation hardness study, it can be seen how there were no long-term damages to the device and that the electrical and sensing performances was not affected by the quantity of absorbed total dose up to 300Gy.

- Pristine versus after X-Ray transfer characteristics show that after 42 hours of storage in dark the sample has completely recovered from the short-term damages.
- The graph of variation versus total dose exhibits a good conservation of the parameters values: mobility and V_{TH} have suffered a small percentage loss, while photocurrent is still at 70% after 300 Gy of irradiation.

Qualitatively, each TIPS-Pn OFET responds adequately to the X-Ray exposure, which is confirmed by the good values of sensitivity. What differentiates the two samples is the organic semiconductor (TIPGe-Pn and TIPS-Pn) and the dielectric layer deposition: both dielectric layers are in aluminum oxide Al_2O_3, but TIPGe-Pn has been built by depositing the first 30nm through aluminum anodizing and the last 70nm through evaporation, while the dielectric of TIPS-Pn has been deposited only through evaporation. This fabrication difference has led to important divergent performances, on both the electrical and X-Ray exposure study, as previously explained.
It is important to emphasize the incontrovertible advantages of flexibility, lightness, low-cost and low energy requirement intrinsic of these devices, as much as the human tissue equivalence in terms of radiation absorption.

To examine more thoroughly OFETs performances in their entirety, higher sensitivity values should be tested for lower dose rates. Resistance over time of these devices could be tested, observing how their parameters (especially mobility and sensitivity) vary in relation to different conservation environments and different quantity of absorbed radiation. Finally, it should also be conducted another radiation hardness study over the same samples after a few weeks or months, in order to establish how their radiation tolerance varies over the time.

Appendix A

Uncertainties calculation

To estimate at best the uncertainties of the calculated parameters, an error propagation has been done on each, following the statistical error propagation, as explained below. The statistical error is a measurement error, which can affect with the same probability, increasing or decreasing the measured value. Every uncertainty has been represented with the standard deviation of values. Here are some definitions which lead to the correct standard deviation formula.

Waste definition

A series of measurements x_1, x_2, ..., x_N is carried out and the mean value is calculated as $\mathrm{x}_\mathrm{m} = \frac{x_1+\cdots+x_\mathrm{N}}{N}$. The waste ξ is defined as the difference between the mean value and the value of a single measurement:

$$\xi_\mathrm{k} = x_\mathrm{k} - x_\mathrm{m}. \tag{A.1}$$

Sample variance definition

The sample variance is defined as the arithmetic mean of the deviations square:

$$S_\mathrm{N}{}^2 = \frac{(\xi_1)^2 + (\xi_2)^2 + \cdots + (\xi_\mathrm{N})^2}{N} = \frac{(x_1 - x_\mathrm{m})^2 + \cdots + (x_\mathrm{N} - x_\mathrm{m})^2}{N}. \tag{A.2}$$

Standard deviation definition

The standard deviation is the positive square root of the sample variance:

$$\sigma = \sqrt{S_\mathrm{N}{}^2} = \sqrt{\frac{(\xi_1)^2 + (\xi_2)^2 + \cdots + (\xi_\mathrm{N})^2}{N}} \tag{A.3}$$

For a large enough number of measurements, the standard variation best represents the absolute error, and it is therefore of fundamental importance to correctly determine the extent of the fluctuations of a measurement.

Complete electrical characterization

In the next pages there is reported the complete electrical characterization for every OFET of the two samples TIPGe-Pn and TIPS-Pn. The following graphs are: (a) the output characteristic, showing the different values of V_{GS}; (b) the transfer characteristic in saturation region; (c) the transfer characteristic in linear region, showing the different curves of I_G and I_D; (d) the transfer characteristic in saturation region, showing the different curves of I_G and I_D, on a logarithmic scale; (e) the transfer characteristic in linear region, showing the different curves of I_G and I_D, on a logarithmic scale.

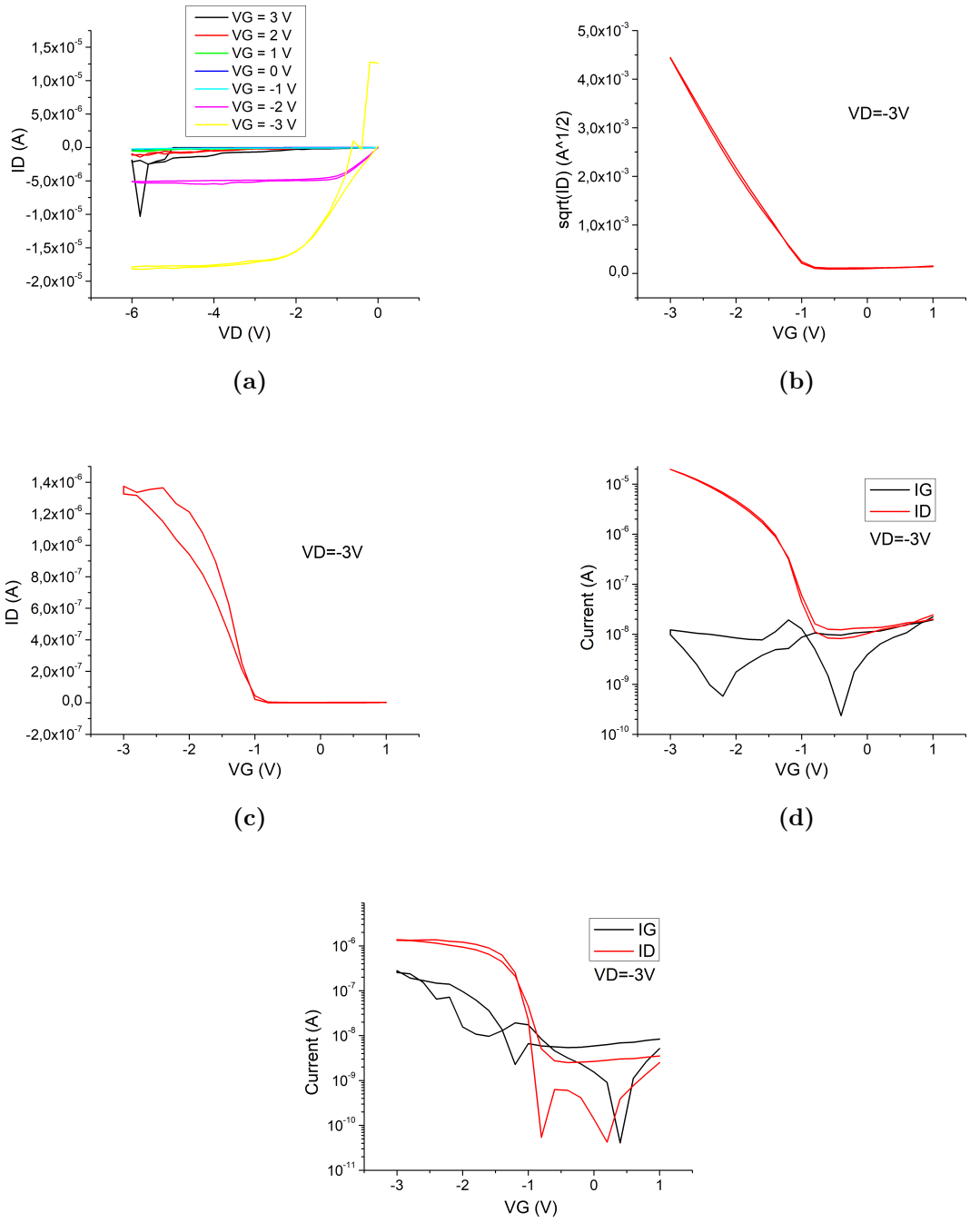

Figure A.1: TIPGe-Pn OFET1

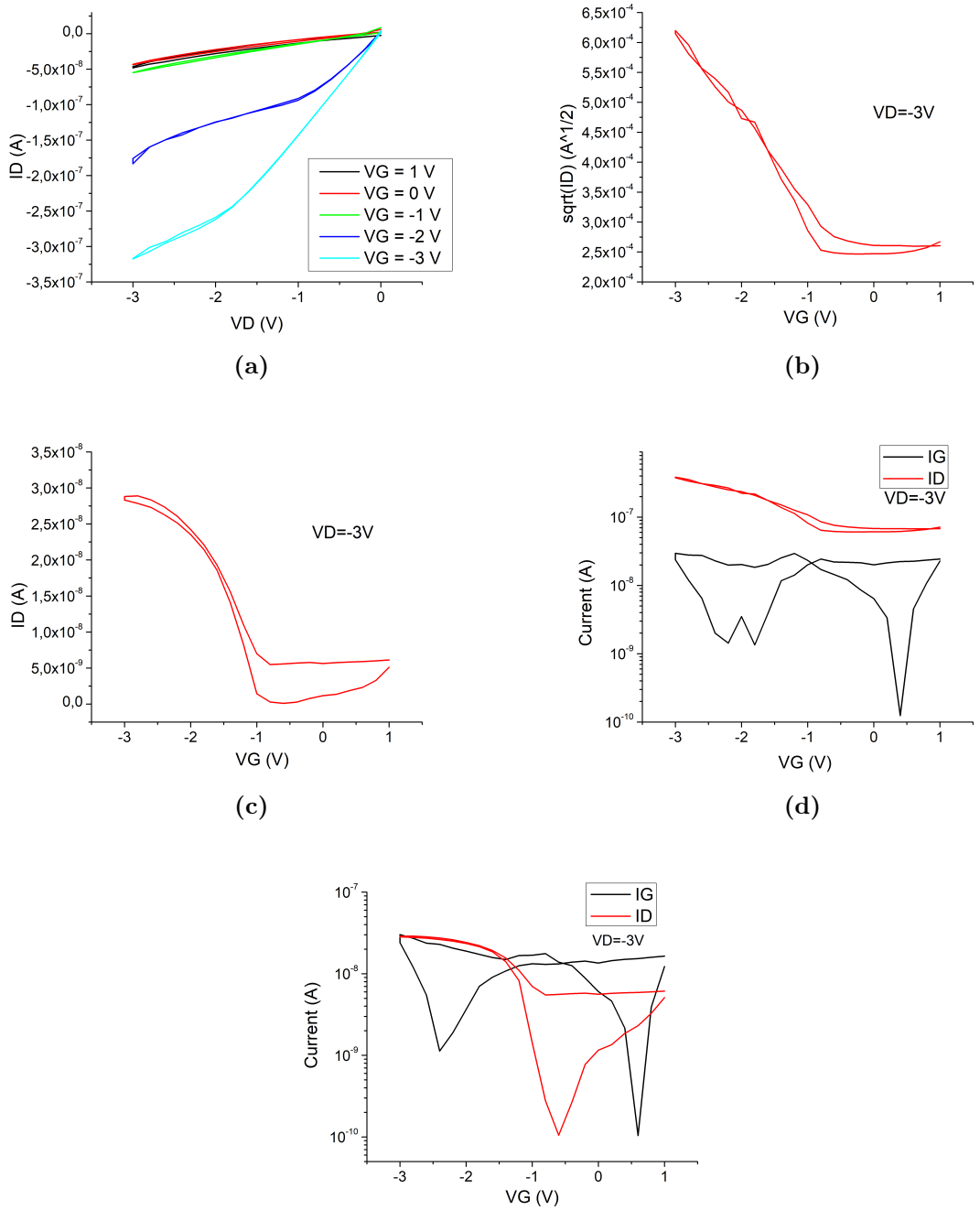

Figure A.2: TIPGe-Pn OFET2

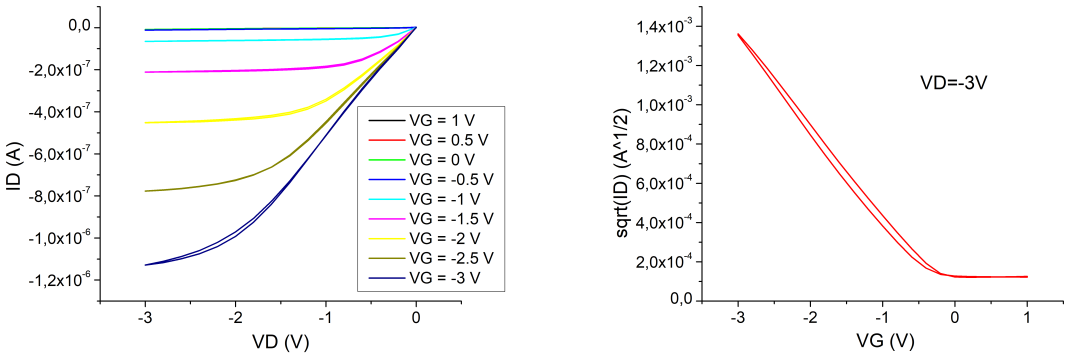

(a)

(b)

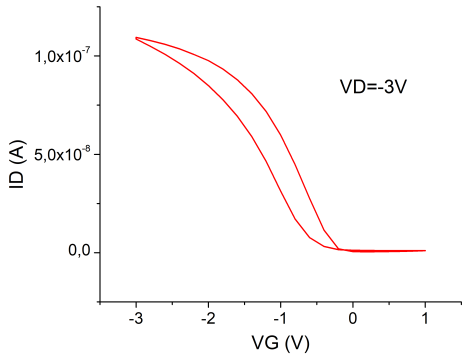

(c)

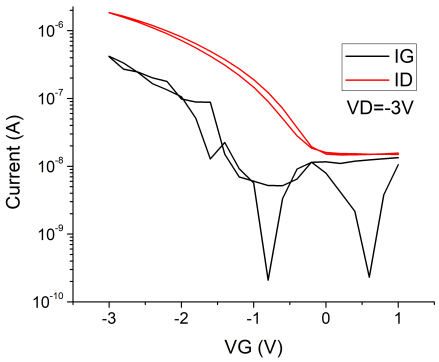

(d)

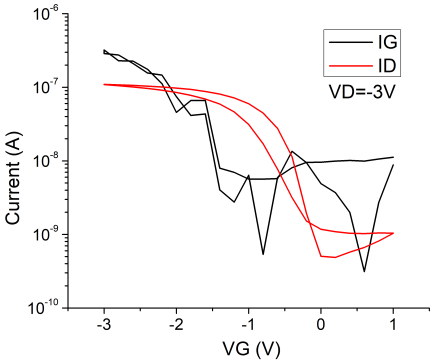

(e)

Figure A.3: TIPGe-Pn OFET3

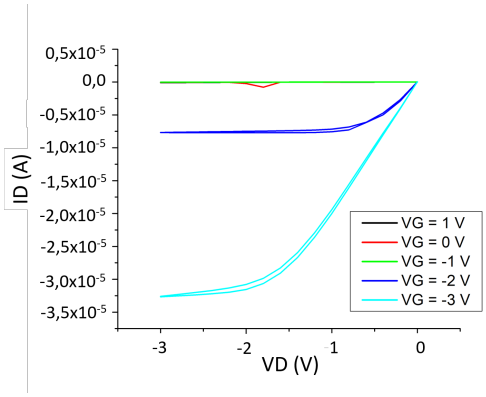

(a)

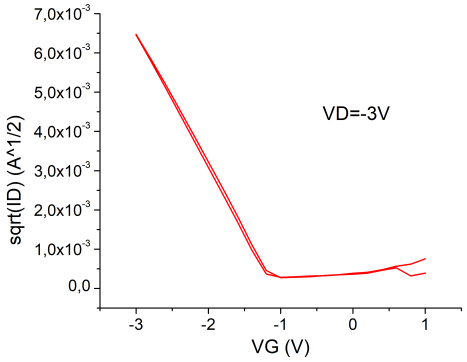

(b)

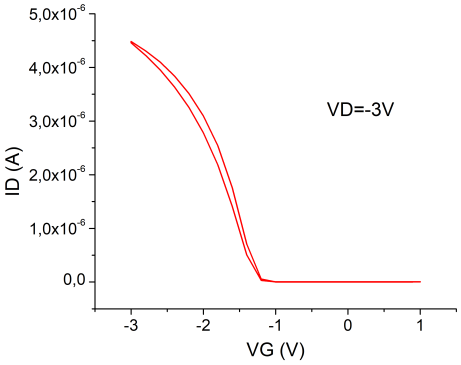

(c)

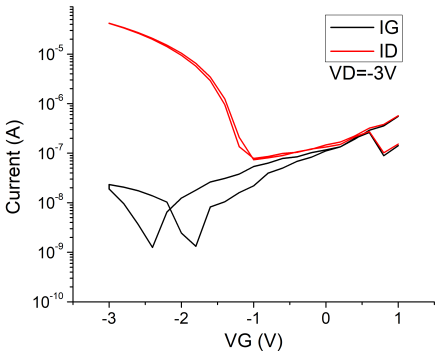

(d)

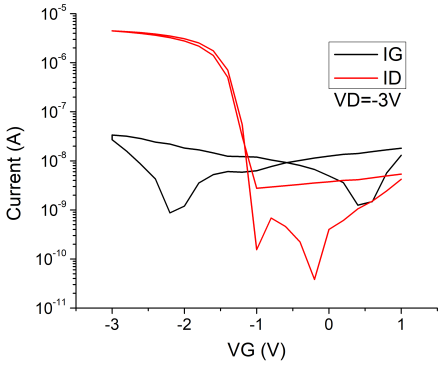

(e)

Figure A.4: TIPS-Pn OFET 2

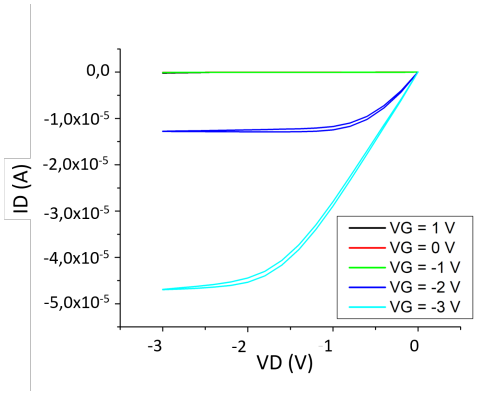

(a)

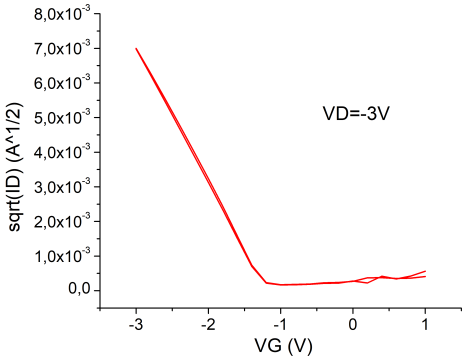

(b)

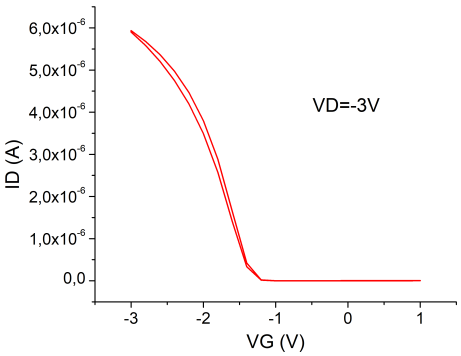

(c)

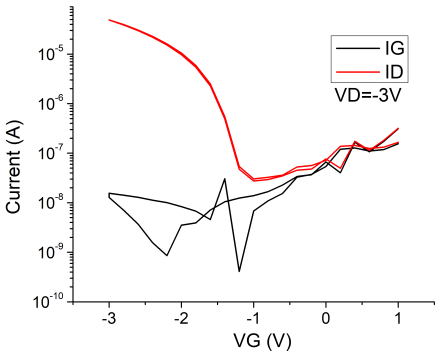

(d)

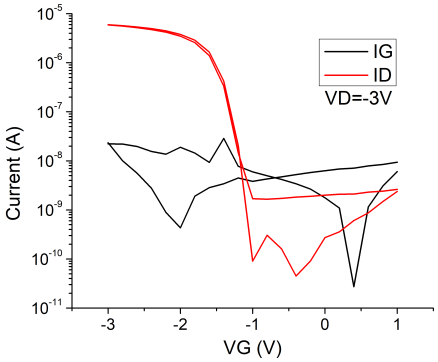

(e)

Figure A.5: TIPS-Pn OFET 3

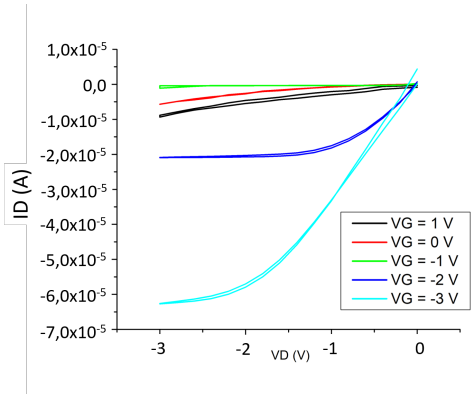

(a)

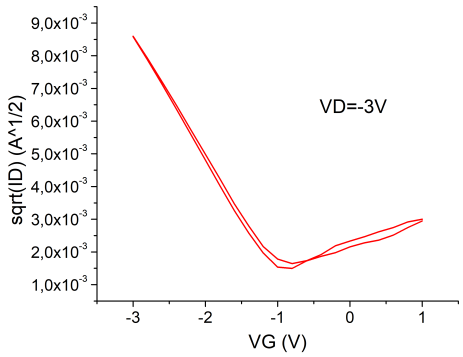

(b)

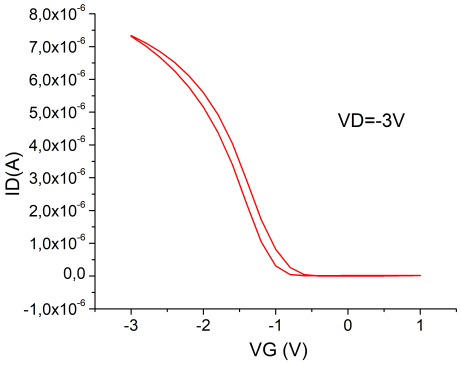

(c)

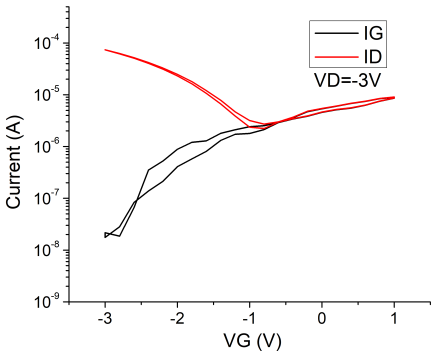

(d)

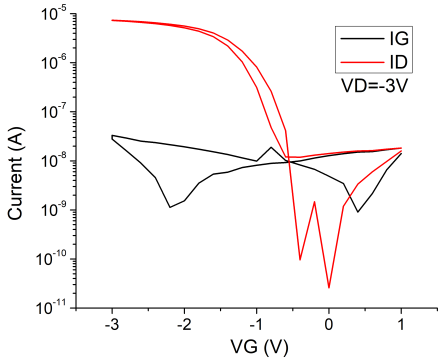

(e)

Figure A.6: TIPS-Pn OFET 4

In Tab.A.1 and Tab.A.2 the mobility, threshold voltage, V_{ON}, ON/OFF ratio and subthreshold swing slope S values are reported with the respective uncertainty for each OFET of each sample.

TIPGe-Pn	**Mobility μ** ($\frac{cm^2}{Vs}$)	**V_{TH} (V)**	**V_{ON} (V)**	**ON/OFF**	**S** ($\frac{V}{decade}$)
OFET 1	$(9.0\pm0.5)\cdot10^{-3}$	-1.0±0.6	-0.8±0.3	2362±1126	0.3±0.4
OFET 2	$(0.9\pm0.5)\cdot10^{-4}$	0.3±0.6	-0.8±0.3	6±1126	1.62±0.05
OFET 3	$(0.4\pm0.5)\cdot10^{-3}$	-0.8±0.6	-0.2±0.3	126±1126	0.75±0.04
OFET 4	$(9.7\pm0.5)\cdot10^{-3}$	-0.3±0.6	-0.2±0.3	221±1126	0.57±0.07

Table A.1: Parameters calculated through electrical characterization for TIPGe-Pn.

TIPS-Pn	**Mobility μ** ($\frac{cm^2}{Vs}$)	**V_{TH} (V)**	**V_{ON} (V)**	**ON/OFF**	**S** ($\frac{V}{decade}$)
OFET 1	$(1.8\pm0.5)\cdot10^{-2}$	-1.0±0.2	-0.8±0.1	2990±1305	0.2±0.4
OFET 2	$(2.1\pm0.5)\cdot10^{-2}$	-1.1±0.2	-1.0±0.1	568±1305	0.3±0.5
OFET 3	$(2.8\pm0.5)\cdot10^{-2}$	-1.2±0.2	-1.0±0.1	1620±1305	0.2±0.5
OFET 4	$(2.5\pm0.5)\cdot10^{-2}$	-0.7±0.2	-0.8±0.1	27±1305	0.97±0.05

Table A.2: Parameters calculated through electrical characterization for TIPS-Pn.

Complete X-Ray characterization

The complete characterization through ionizing radiation exposition of TIPGe-Pn and TIPS-Pn based is reported in the next pages. The following graphs represent the comparison between transfer characteristics before and after X-Ray exposure on the TIPGe-Pn OFET 3 (Fig.A.7) and on the TIPS-Pn OFET 2 (Fig.A.8); afterwards, the characteristic curve I_D vs time, for three cycles of X-Ray exposition, each one on 60 seconds of irradiation (t_{ON}) and 60 seconds at rest (t_{OFF}) (Fig.A.9 and Fig.A.10). For the FN20_11_03 sample only OFET 1 and 3 have been characterized.

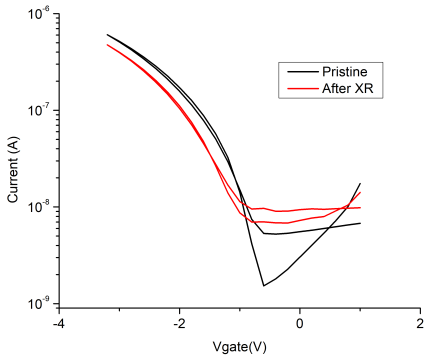

(a) Transfer characteristics in saturation regime on a logarithmic scale

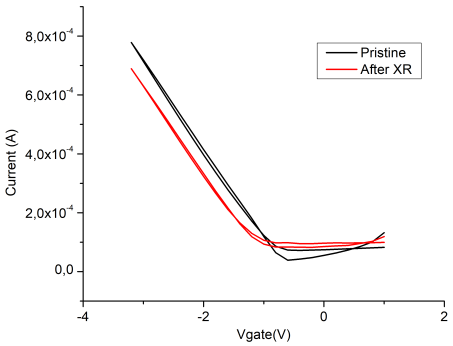

(b) Transfer characteristics in saturation regime on a linear scale

Figure A.7: TIPGe-Pn OFET 3

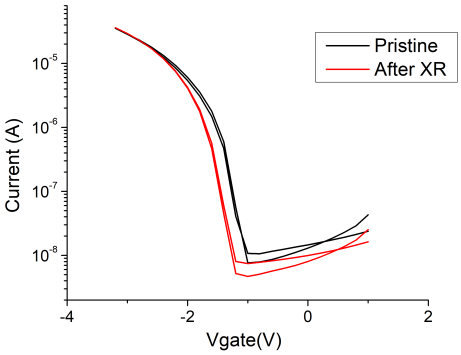

(a) Transfer characteristics in saturation regime on a logarithmic scale

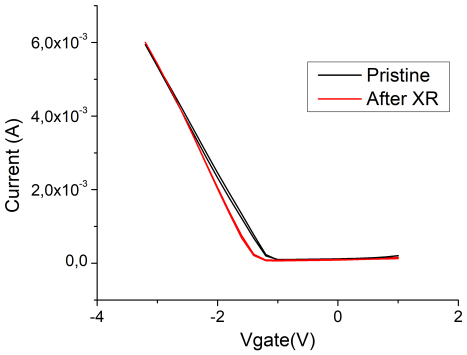

(b) Transfer characteristics in saturation regime on a linear scale

Figure A.8: TIPS-Pn OFET 2

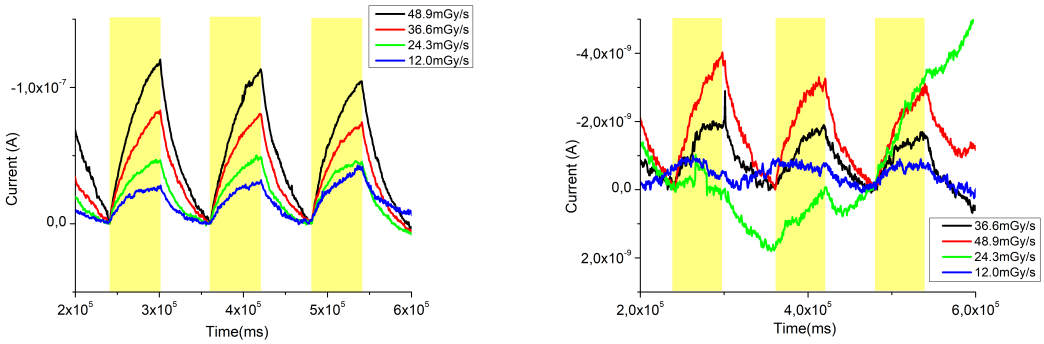

(a) OFET 1 **(b)** OFET 3

Figure A.9: TIPGe-Pn

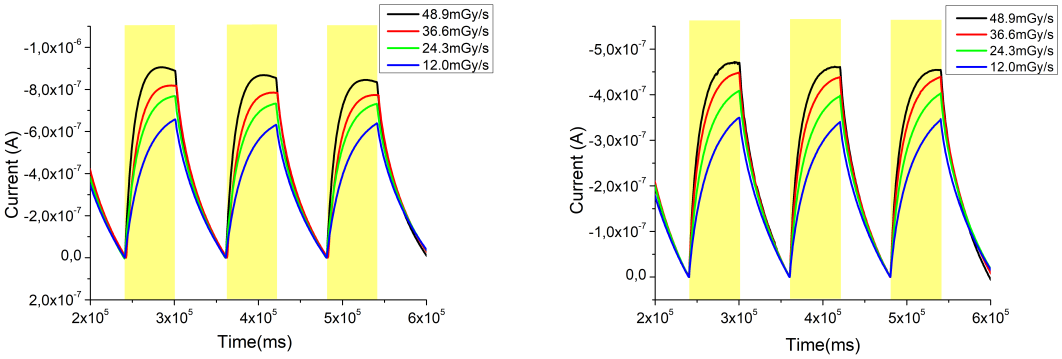

(a) OFET 2 **(b)** OFET 3

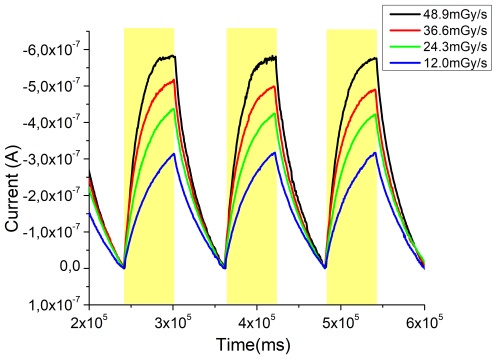

(c) OFET 4

Figure A.10: TIPS-Pn

Bibliography

[1] Ioannis Kymissis. *Organic field effect transistors: theory, fabrication and characterization*. Springer Science & Business Media, 2008.

[2] L. Sim, Voo Tin Vui Richard, and Mariatti Jaafar. Properties of epoxy nanocomposite thin films prepared by spin coating technique. *Journal of Plastic Film and Sheeting*, 27:331 – 346, 09 2011. doi: 10.1177/8756087911419745.

[3] Edward Bormashenko, Yelena Bormashenko, and Mark Frenkel. Formation of hierarchical porous films with breath-figures self-assembly performed on oil-lubricated substrates. *Materials*, 12:3051, 09 2019. doi: 10.3390/ma12183051.

[4] Antonio Sánchez-Herencia. Water based colloidal processing of ceramic laminates. *Key Engineering Materials - KEY ENG MAT*, 333:39–48, 03 2007. doi: 10.4028/www.scientific.net/KEM.333.39.

[5] Jaewon Oh, Jung-Yeul Jung, Kyounghwan Song, Youngsuk Nam, Ki-Young Sung, Seungtae Oh, and Jaehwan Shim. Characteristics analysis of the developed surface modification technologies to improve the anti-corrosion performances for offshore equipments. *Journal of Mechanical Science and Technology*, 33, 08 2019. doi: 10.1007/s12206-019-0742-y.

[6] Matthew Sykes. Circumventing the tradeoff between optical absorption and exciton diffusion in organic photovoltaics. 01 2015.

[7] E Shim. Bonding requirements in coating and laminating of textiles. In *Joining Textiles*, pages 309–351. Elsevier, 2013.

[8] Ying Diao, Leo Shaw, Zhenan Bao, and Stefan CB Mannsfeld. Morphology control strategies for solution-processed organic semiconductor thin films. *Energy & Environmental Science*, 7(7):2145–2159, 2014.

[9] Zachary A Lamport, Hamna F Haneef, Sajant Anand, Matthew Waldrip, and Oana D Jurchescu. Tutorial: Organic field-effect transistors: Materials, structure and operation. *Journal of Applied Physics*, 124(7):071101, 2018.

[10] Shuming Duan, Tao Wang, Bowen Geng, Xiong Gao, Chenguang Li, Jing Zhang, Yue Xi, Xiaotao Zhang, Xiaochen Ren, and Wenping Hu. Solution-processed centimeter-scale highly aligned organic crystalline arrays for high-performance organic field-effect transistors. *Advanced Materials*, 32(12):1908388, 2020.

[11] Matthew James Griffith, Sophie Cottam, Joshua Stamenkovich, Jessie A Posar, and Marco Petasecca. Printable organic semiconductors for radiation detection: from fundamentals to fabrication and functionality. *Frontiers in Physics*, 8:22, 2020.

[12] Martin Egginger, Siegfried Bauer, Reinhard Schwödiauer, Helmut Neugebauer, and Niyazi Serdar Sariciftci. Current versus gate voltage hysteresis in organic field effect transistors. *Monatshefte für Chemie-Chemical Monthly*, 140(7):735–750, 2009.

[13] Yong Xu, Yun Li, Songlin Li, Francis Balestra, Gérard Ghibaudo, Wenwu Li, Yen-Fu Lin, Huabin Sun, Jing Wan, Xinran Wang, et al. Precise extraction of charge carrier mobility for organic transistors. *Advanced Functional Materials*, 30(20): 1904508, 2020.

[14] Marcia Dutra R Silva. Ionizing radiation detectors. *Evolution of Ionizing Radiation Research*, pages 189–209, 2015.

[15] Laura Basirico, Andrea Ciavatti, Tobias Cramer, Piero Cosseddu, Annalisa Bonfiglio, and Beatrice Fraboni. Direct x-ray photoconversion in flexible organic thin film devices operated below 1 v. *Nature communications*, 7(1):1–9, 2016.

[16] Laura Basiricò, Andrea Ciavatti, Ilaria Fratelli, Diego Dreossi, Giuliana Tromba, Stefano Lai, Piero Cosseddu, Annalisa Bonfiglio, Francesco Mariotti, Carlo Dalla Val, et al. Medical applications of tissue-equivalent, organic-based flexible direct x-ray detectors. *Frontiers in Physics*, 8:13, 2020.

[17] Stefano Lai, Piero Cosseddu, Laura Basiricò, Andrea Ciavatti, Beatrice Fraboni, and Annalisa Bonfiglio. A highly sensitive, direct x-ray detector based on a low-voltage organic field-effect transistor. *Advanced Electronic Materials*, 3(8):1600409, 2017.

[18] Inés Temiño, Laura Basiricò, Ilaria Fratelli, Adrián Tamayo, Andrea Ciavatti, Marta Mas-Torrent, and Beatrice Fraboni. Morphology and mobility as tools to control and unprecedentedly enhance x-ray sensitivity in organic thin-films. *Nature communications*, 11(1):1–10, 2020.

[19] Andrew M Zeidell, Tong Ren, David S Filston, Hamna F Iqbal, Emma Holland, J Daniel Bourland, John E Anthony, and Oana D Jurchescu. Organic field-effect transistors as flexible, tissue-equivalent radiation dosimeters in medical applications. *Advanced Science*, 7(18):2001522, 2020.

[20] Christian Poivey. Radiation hardness assurance for space systems. In *IEEE NSREC Short Course*, pages V1–V57, 2002.

[21] DM Fleetwood and HA Eisen. Total-dose radiation hardness assurance. *IEEE Transactions on Nuclear Science*, 50(3):552–564, 2003.

[22] R.L. Pease, W.E. Combs, A. Johnston, T. Carriere, C. Poivey, A. Gach, and S. McClure. A compendium of recent total dose data on bipolar linear microcircuits. In *1996 IEEE Radiation Effects Data Workshop. Workshop Record. Held in conjunction with The IEEE Nuclear and Space Radiation Effects Conference*, pages 28–37, 1996. doi: 10.1109/REDW.1996.574185.

[23] Kiril Sakovsky. Radiation Hardness Testing for Space Application Electronic Devices. `https://www.dimacred.com/wp-content/uploads/2018/06/RadiationHardnessResearch.pdf`, 2012.

[24] Stefano Lai, Giulia Casula, Pier Carlo Ricci, Piero Cosseddu, and Annalisa Bonfiglio. All-organic, low voltage, transparent and compliant organic field-effect transistor fabricated by means of large-area, cost-effective techniques. *Applied Sciences*, 10(19):6656, 2020.

[25] Andrea Ciavatti, Laura Basiricò, Ilaria Fratelli, Stefano Lai, Piero Cosseddu, Annalisa Bonfiglio, John E Anthony, and Beatrice Fraboni. Boosting direct x-ray detection in organic thin films by small molecules tailoring. *Advanced Functional Materials*, 29(21):1806119, 2019.

Ringraziamenti

Vorrei ringraziare innanzitutto mamma e papà, che nonostante i battibecchi mi sono sempre stati accanto e mi hanno sempre supportata, sopportata e amata.
Ringrazio tutta la mia famiglia, la nonna, i numerosi zii e cugini, per l'affetto e il sostegno che anche da lontano siete stati capaci di darmi.
Ringrazio i miei ex compagni di corso e amici Stefano, Giovanni, Chiara, Viviana, Gianmarco e Janko, per avermi accompagnata in questi anni, per il supporto, le risate e le belle serate.
Ringrazio il gruppo di amici di Lucrezia, siete tanti e mi siete mancati tutti nei mesi passati a Bologna. Nonostante la distanza mi fate sempre sentire a casa.
Ringrazio le coinquiline di questi anni, tutte mi hanno insegnato qualcosa e hanno rallegrato la quotidianità anche nei momenti più difficili.
Ringrazio la Prof.ssa Beatrice Fraboni, le Dott.sse Laura Basiricò e Ilaria Fratelli, per avermi seguita, guidata ed avermi insegnato tanto.
Ringrazio Davide, anche se non ci vediamo da tanto mi sei sempre stato vicino, mi hai regalato risate e speranza.
Ringrazio Matilde e Samuele, per l'affetto e le indimenticabili serate passate con voi.
Ringrazio Lisa e Stella, siete la mia felicità e salvezza. Grazie per ogni prezioso momento passato insieme, siete indelebili.
Un ringraziamento speciale va a Samuele, che mi ha accompagnata, aiutata, amata ed ha creduto in me sempre. Non dimenticherò mai questi anni ed in gran parte è merito tuo.
Infine, ringrazio mio nonno Franco, per avermi guidata con la sua saggezza ed amata immensamente. Questa tesi è dedicata a lui, che rimarrà per sempre nel mio cuore e nei miei pensieri.